frontiers | Frontiers in Materials

TYPE Original Research
PUBLISHED 09 May 2024
DOI 10.3389/fmats.2024.1357094



OPEN ACCESS

EDITED BY
Chaopeng Xie,
North China University of Water Conservancy and Electric Power, China

REVIEWED BY
Wanhui Feng,
Zhongkai University of Agriculture and Engineering, China
Ibrahim Saad Agwa,
Suez University, Egypt

*CORRESPONDENCE
Naraindas Bheel,
naraindas04@gmail.com
Taoufik Najeh,
taoufik.najeh@ltu.se

RECEIVED 17 December 2023
ACCEPTED 02 April 2024
PUBLISHED 09 May 2024

CITATION
Abdullah GMS, Chohan IM, Ali M, Bheel N, Ahmad M, Najeh T, Gamil Y and Almujibah HR (2024), Effect of titanium dioxide as nanomaterials on mechanical and durability properties of rubberised concrete by applying RSM modelling and optimizations.
*Front. Mater.* 11:1357094.
doi: 10.3389/fmats.2024.1357094



# Effect of titanium dioxide as nanomaterials on mechanical and durability properties of rubberised concrete by applying RSM modelling and optimizations

Gamil M. S. Abdullah[1], Imran Mir Chohan[2], Mohsin Ali[3], Naraindas Bheel[4]*, Mahmood Ahmad[5,6], Taoufik Najeh[7]*, Yaser Gamil[8] and Hamad R. Almujibah[9]

[1]Department of Civil Engineering, College of Engineering, Najran University, Najran, Saudi Arabia, [2]Department of Mechanical Engineering, Universiti Teknologi PETRONAS, Bandar Seri Iskandar, Malaysia, [3]Graduate School of Urban Innovation, Department of Civil Engineering, Yokohama National University, Kanagawa, Japan, [4]Department of Civil and Environmental Engineering, Universiti Teknologi PETRONAS, Bandar Seri Iskandar, Malaysia, [5]Institute of Energy Infrastructure, Universiti Tenaga Nasional, Kajang, Malaysia, [6]Department of Civil Engineering, University of Engineering and Technology Peshawar (Bannu Campus), Bannu, Pakistan, [7]Operation and Maintenance, Operation, Maintenance and Acoustics, Department of Civil, Environmental and Natural Resources Engineering, Luleå University of Technology, Luleå, Sweden, [8]Department of Civil Engineering, School of Engineering, Monash University Malaysia, Jalan Lagoon Selatan, Selangor, Malaysia, [9]Department of Civil Engineering, College of Engineering, Taif University, Taif, Saudi Arabia

The use of rubber aggregates derived from discarded rubber tyres in concrete is a pioneering approach to replacing natural aggregate (NA) and promoting sustainable building practices. Recycled aggregate in concrete serves the dual purpose of alleviating the accumulation of discarded rubber tyres on the planet and providing a more sustainable alternative to decreasing natural aggregate. Due to fact that the crumb rubber (CR) decreases the strength when used in concrete, incorporating titanium dioxide ($TiO_2$) as a nanomaterial to counteract the decrease in strength of crumb rubber concrete is a potential solution. Response Surface Methodology was developed to generate sixteen RUNs which contains different mix design by providing two input parameters like $TiO_2$ at 1%, 1.5%, and 2% by cement weight and CR at 10%, 20%, and 30% as substitutions for volume of sand. These mixtures underwent testing for 28 days to evaluate their mechanical, deformation, and durability properties. Moreover, the compressive strength, tensile strength, flexural strength and elastic modulus were recorded by 51.40 MPa, 4.47 MPa, 5.91 MPa, and 40.15 GPa when 1.5% $TiO_2$ and 10% CR were added in rubberised concrete after 28 days respectively.

**Abbreviations:** CR, Crumb Rubber; UV, Ultraviolet; $TiO_2$, Titanium Dioxide; SG, Specific Gravity; RSM, Response Surface Methodology; CA, Coarse Aggregate; RA, Rubber Aggregates; SP, Superplasticizer; NA, Natural Aggregate; CCD, Central Composite Design; MPa, Mega Pascal; DS, Drying Shrinkage; GPa, Giga Pascal; AP, Apparent Porosity; PC, Portland Cement; ANOVA, Analysis Of Variance; CS, Compressive Strength; UTM, Universal Testing Machine; TS, Tensile Strength; JSCE, Japan Society of Civil Engineers; FS, Flexural Strength; LVTD, Longitudinal Variable Displacement Transducer; ME, Modulus of Elasticity; $Ca(OH)_2$, Calcium Hydroxide; NaOH, Sodium Hydroxide; ITZ, Interficial Transition Zone; -S-H, Calcium Silicate Hydrates; SMSS, Sequential Model Sum of Squares.

Furthermore, the incorporation of $TiO_2$ led to reduced drying shrinkage and sorptivity in rubberized concrete, especially with increased $TiO_2$ content. The study highlights that $TiO_2$ inclusion refines pore size and densifies the interface between cement matrix and aggregate in hardened rubberized concrete. This transformative effect results in rubberized concrete demonstrating a commendable compressive strength comparable to normal concrete.

KEYWORDS

**crumb rubber, concrete, drying shrinkage, mechanical and durability characteristics, multi-objective RSM modelling, titanium dioxide**

# 1 Introduction

Every year, enormous amounts of scrap tires are discarded globally, with the United States, Turkey, and the European Union alone generating an average of 250 million, 10 million, and 3.4 million tons, respectively (Onuaguluchi and Panesar, 2014; Demir et al., 2015; Mohammed et al., 2016). An annual global concern has emerged regarding the improper disposal of more than 500 million waste tires after they have outlived their usefulness (Thomas et al., 2016). He immediate concern surrounding this concerning increase stems from the direct and indirect risks it poses to human wellbeing, ecological integrity, and safety (Chohan et al., 2023). In addition to promoting rodent infestation, disposing of these tires in landfills and dumpsites presents a sustained challenge due to the sluggish biodegradation process that contributes to environmental risks, especially during fire (Pelisser et al., 2011). As a viable remedy to this problem, the reprocessing of used tyres into crumb rubber (CR) for concrete has emerged. This novel methodology not only facilitates the restoration of ecological equilibrium but also possesses considerable economic merit (Guo et al., 2014).

CR extracted from the exterior surface of tire scraps, is employed as a partial substitute for sand in Portland cement (PC) concrete, resulting in what is generally defined as CR concrete, or rubberized concrete. This innovative concrete variant boasts several advantages over traditional concrete, including reduced density (Demir et al., 2015; Mohammed et al., 2016), enhanced ductileness (Shu and Huang, 2014), improved plastic capacity (Mohammed et al., 2011), heightened robustness (Mohammed, 2010), increased impact resistance (Ganjian et al., 2009), superior resistance to infiltration (Bravo and De Brito, 2012), lower thermal conductivity (Li et al., 2004) and enhanced electrical resistivity (Onuaguluchi and Panesar, 2014). Additionally, rubberized concrete is recognized for its superior durability (Youssf et al., 2014). Despite these advantages, rubberized concrete does face certain drawbacks, notably a decline in compressive, tensile, flexural, and splitting strengths, additionally Young's modulus, with an increasing proportion of CR replacing fine aggregate. The reduced strength can be accredited to the inadequate bond between PC matrix and CR constituent part, which is a result of the hydrophobic characteristics of CR introduced during tire manufacturing with zinc stearate (Youssf et al., 2014). The ability of CR to repel water generates an airtight, non-polar layer, which increases the dimension ITZ between PC matrix and CR constituent part. The presence of a denser region undermines the integrity of the bond, concentrates strain, and ultimately results in the formation of microscopic fissures, which prematurely fail (Mohammed et al., 2012; Sadek and El-Attar, 2015; Li G. et al., 2016; Thomas et al., 2016).

To expand the practical usage and acceptance of CR concrete in construction, efforts have been focused on boosting its strength. Researchers have explored various surface treatment methods for crumb rubber (CR) particles to augment connection between CR and PC mixture. It was conducted experiments to evaluate several methods for treating surfaces, such as water, a carbon tetrachloride solution, and an adhesive admixture cleaner. The findings indicated that the compressive strength (CS) exhibited an increase of up to 57% in comparison to the reference mixture (Rostami et al., 2000). Researchers found success using aqueous NaOH to treat CR surfaces, improving the bond and subsequently elevating strengths (Segre and Joekes, 2000). However, Researchers did not witness significant mechanical strength improvements despite treating CR with NaOH and silane coupling agents (Albano et al., 2005). Authors explored the partial oxidation of CR to create hydrophilic groups, strengthening the bond with the cement matrix, albeit at an increased cost (Chou et al., 2010). It was noticed that the combined NaOH treatment with silica fume in rubberized concrete, noting a reduced strength reduction compared to untreated rubberized concrete (Pelisser et al., 2011). It was found that adding limestone powder, silica fume, and superplasticizer admixtures made the concrete stronger, but not as strong as regular concrete (Corinaldesi et al., 2011; Turki et al., 2012). Huang et al. (Huang B. et al., 2013) and Dong et al. (Dong et al., 2013) experimented with two-phase treatment for surface, finding that employing both stages was more effective in strengthening rubberized concrete. Meddah et al. (Meddah et al., 2014) attempted NaOH treatment and adding fine aggregate to roughen CR's surface, but this method did not improve concrete strength significantly. Li et al. (Li G. et al., 2016) did a study where they used silane coupling agents and carboxylate styrene-butadiene rubber latex to treat used tire fibers. They saw improvements in the materials' CS and FS. However, different findings from (Dong et al., 2013; Shu and Huang, 2014) suggest that CR treatment methods might not always make rubberized concrete as strong as regular concrete. This makes it less useful in construction because it is not as strong as regular concrete.

Advancements in nanotechnology offer promising prospects for material development at the nanoscale, enabling precise manipulation of matter at atomic levels. Nano-engineered materials exhibit superior performance with respect to their larger-scale counterparts due to their nano-sized dimensions (Nik et al., 2010;

Bahari et al., 2016; Faried et al., 2021; Mousavi et al., 2021). Within the construction sector, the emergence of titanium dioxide ($TiO_2$) as a nanomaterial has addressed the demand for high-performance materials at a competitive cost. $TiO_2$ nanoparticles, also known as Titania, have gained popularity in composites (cementitious) owing to their enhanced photochemical activity, stability, and cost-effectiveness (Nik and Bahari, 2012; Yousefi et al., 2013; Li Q. et al., 2016; Loh et al., 2018). The inclusion of nanoparticles, such as titanium, expedites the hydration process by filling microscale voids and providing sites for the early formation of hydration products (Amiri et al., 2012; Bahari et al., 2012; 2015). Studies have shown compelling results regarding the benefits of incorporating titanium nanoparticles into cementitious matrix (Abu el-Hassan et al., 2023; Ghanim et al., 2023). Consequently, Meng et al. (Meng et al., 2012) identified a 45% increase in early-age compressive strength by adding 0.05% titanium nanoparticles to cement, attributing this enhancement to accelerated C-S-H formation and pore reduction. Jayapalan et al. (Jayapalan et al., 2009) talked about how titanium nanoparticles help create nucleation sites in cement hydration products, which speeds up reactions by lowering energy barriers. Zhang et al. (Zhang R. et al., 2015) confirmed significant enhancements in CS and pore refinement in PC mortar due to the addition of titania nanoparticles, linked to accelerated cement hydration. Feng et al. (Feng et al., 2013) observed that cement paste with Titania nanoparticles had higher flexural strength. They said this was because the needle-shaped nanoparticles made the microstructure better, with fewer holes and more compact, smoother microcracks. The use of $TiO_2$ in rubberised concrete has several benefits, such as heightened mechanical characteristics, including augmented CS and FS, as well as enhanced toughness, resulting in more durable buildings. In addition, the use of $TiO_2$ improves the durability of rubberised composite by reducing water absorption and enhancing resistance to chemical degradation and freeze-thaw cycles, thus prolonging its service life. The material's photocatalytic qualities allow for self-cleaning abilities, effectively fighting surface pollutants and preserving cleanliness. Additionally, it offers UV resistance, protecting against deterioration caused by exposure to sunshine. In addition, the use of $TiO_2$ in rubberised composite augments its flow of fresh mix and decreases friction during the mixing process. This, in turn, allows for simpler placement and finishing of the concrete, resulting in smoother surfaces and better-quality buildings. In summary, incorporating $TiO_2$ into rubber concrete not only improves its performance and durability but also promotes sustainability by using recycled rubber and minimising environmental harm.

Furthermore, utilising RSM as an optimisation technique to investigate the characteristics of rubberised concrete provides clear benefits compared to other methods. When compared to methods like the Taguchi method, RSM is more efficient because it can give useful results with fewer experimental runs. This streamlines the research process and preserves resources. In addition, RSM's adaptability in modelling allows for the representation of detailed, non-linear connections between input variables and output responses, which is essential for comprehending the intricate nature of concrete qualities. Furthermore, RSM's emphasis on local optimisation enables precise revisions towards optimum solutions, which is especially advantageous in concrete research where little modifications may greatly impact results. The interpretability of RSM models boosts their value by enabling investigators to differentiate the impact of individual components and their interactions on certain attributes. By combining RSM with well-crafted experimental designs, one may guarantee a methodical investigation of the design space, resulting in dependable and practical outcomes. In summary, RSM proves to be a reliable and effective technique for optimising the characteristics of rubberised concrete. It provides a well-rounded approach that combines modelling flexibility, experimental efficiency, and interpretative capability. There are many experimental investigations performed on the $TiO_2$ as nanomaterials (Al-Rbaihat and Al-Marafi, 2023; Bunea et al., 2023; Mostafa et al., 2023; Rawat et al., 2023) and CR as replacement for sand in concrete individually (Shahjalal et al., 2023; Youssf et al., 2023; Aghamohammadi et al., 2024) but there is very limited research were accomplished on rubberised concrete mixed with $TiO_2$ as nanoscale particle. Therefore, this study aims to experimentally explore the integration of titanium dioxide as a nanomaterial into rubberized concrete. The goal is to perform an optimization framework using RSM and to look at the material's mechanical characteristics (tensile, compressive, and flexural strengths), deformation characteristics (modulus of elasticity and drying shrinkage), and durability aspects (sorptivity and porosity).

# 2 Experimental program

## 2.1 Materials

The major binding ingredient utilized in research work was Portland cement (PC), which conformed to ASTM C150/C150-16e1 (2016) requirements and had a specific gravity (SG) of 3.15. The river sand was employed as a fine aggregate, passing from a 4.75 mm mesh with a SG of around 2.65. Crushed stone, with a size of 20 mm, was employed as a coarse aggregate (CA), with an SG of about 2.60. Moreover, crumb rubber (CR), characterized by a SG of 0.92 and passed through a 1.18 mm sieve, was used as a partial substitution for sand at volumes of 10%, 20%, and 30% in this investigation. Incorporation of $TiO_2$ powder as a nanomaterial in rubberized concrete was a crucial aspect of the experiment. The average particle size ranged between 10 and 50 nm. To confirm uniform dispersion of nanoscale particles and prevent cohesion or agglomeration when mixed with water, a third-generation superplasticizer was employed (Zhao et al., 2017). To achieve the appropriate ability to flow, a modified polycarboxylate-based superplasticizer (SP) was utilised in the form of a water-based solution to modify the mixes. The substance is in a liquid state and has a pH of 6.2 and a SG of 1.08. Importantly, it contains no chloride ions. Water suitable for drinking and meeting standard quality criteria for concrete mixing was applied in the investigation, maintaining a water-to-cement ratio of 0.35.

## 2.2 Mix proportions generated by RSM

The Design Expert 10 software was used to develop RSM for optimization. Employing the Central Composite Design (CCD)

TABLE 1 Mix Proportions of CR-Concrete blended with $TiO_2$.

| Mix ID | Ingredients (%) | | | | | Mass of constituents utilized in CR concrete (kg/m$^3$) | | | |
|---|---|---|---|---|---|---|---|---|---|
| | $TiO_2$ | CR | PC | $TiO_2$ | CA | Sand | CR | SP | Water |
| M0 | 0.0 | 0.0 | 585 | 0.0 | 1,450 | 675 | 0.0 | 5.79 | 205 |
| M1 | 1.5 | 10 | 576.22 | 8.78 | 1,450 | 630.53 | 44.47 | 5.79 | 205 |
| M2 | 1.0 | 10 | 579.15 | 5.85 | 1,450 | 630.53 | 44.47 | 5.79 | 205 |
| M3 | 1.5 | 30 | 576.22 | 8.78 | 1,450 | 541.59 | 133.41 | 5.79 | 205 |
| M4 | 1.0 | 30 | 579.15 | 5.85 | 1,450 | 541.59 | 133.41 | 5.79 | 205 |
| M5 | 2.0 | 30 | 573.30 | 11.70 | 1,450 | 541.59 | 133.41 | 5.79 | 205 |
| M6 | 1.0 | 10 | 579.15 | 5.85 | 1,450 | 630.53 | 44.47 | 5.79 | 205 |
| M7 | 1.0 | 20 | 579.15 | 5.85 | 1,450 | 586.06 | 88.94 | 5.79 | 205 |
| M8 | 1.5 | 20 | 576.22 | 8.78 | 1,450 | 586.06 | 88.94 | 5.79 | 205 |
| M9 | 1.5 | 20 | 576.22 | 8.78 | 1,450 | 586.06 | 88.94 | 5.79 | 205 |
| M10 | 2.0 | 20 | 573.30 | 11.70 | 1,450 | 586.06 | 88.94 | 5.79 | 205 |
| M11 | 1.5 | 20 | 576.22 | 8.78 | 1,450 | 586.06 | 88.94 | 5.79 | 205 |
| M12 | 2.0 | 20 | 573.30 | 11.70 | 1,450 | 586.06 | 88.94 | 5.79 | 205 |
| M13 | 1.5 | 20 | 576.22 | 8.78 | 1,450 | 586.06 | 88.94 | 5.79 | 205 |
| M14 | 1.5 | 30 | 576.22 | 8.78 | 1,450 | 541.59 | 133.41 | 5.79 | 205 |
| M15 | 1.5 | 20 | 576.22 | 8.78 | 1,450 | 586.06 | 88.94 | 5.79 | 205 |
| M16 | 2.0 | 10 | 573.30 | 11.70 | 1,450 | 630.53 | 44.47 | 5.79 | 205 |

method, the research focused on two key factors: CR and $TiO_2$ as nanomaterials. Each variable underwent testing three times, with CR at 10%, 20%, and 30% volume substitution for sand, and $TiO_2$ at 1%, 1.5%, and 2% addition by weight of PC. This particular approach, previously utilized by researchers (Jo et al., 2015; Al-Fakih et al., 2020; Khed et al., 2020) culminated in 16 distinct mixes. These were generated by the RSM, meticulously exploring numerous Runs of the specified variables outlined in Table 1. Evaluation in the laboratory encompassed examining each mix for its flexural strength (FS), tensile strength (TS), modulus of elasticity (ME), compressive strength (CS), drying shrinkage (DS), sorptivity, and apparent porosity (AP). Moreover, the strength of each mix after a 28-day period was scrutinized. These assessments served as the basis for the RSM study and subsequent optimization of the mixtures. RSM played a pivotal role, not only in scrutinizing the results but also in conducting an analysis of variance (ANOVA) to ensure the reliability of the conducted tests. The study harnessed RSM to discern the most optimal values for the output variables (CS, TS, FS, ME, DS, sorptivity, and AP), factoring in the substantial impact of the input variables ($TiO_2$ and CR) on the overall outcomes.

## 2.3 Sample preparation and testing methods

### 2.3.1 Mixing and casting

The process of creating the specimens involved thorough preparation of rubberized concrete blended with $TiO_2$ as a nanomaterial, following the guidelines specified in BS 1881: Part 125:1986. The procedure started by dry mixing the sand, CA, and CR for 50 s using a concrete mixer. Afterwards, half of the water that was being mixed was added, and the entire mixture was stirred for a duration of 1 min. Besides, PC was thereafter inserted and well blended for an extra minute. To ensure proper dispersion and prevent potential agglomeration of the nanoparticles, $TiO_2$ and superplasticizer were thoroughly mixed with water for 3–5 min using a high-speed stirrer (Younis and Mustafa, 2018; Orakzai, 2021). This step aimed to enhance flow of fresh mix and facilitate uniform distribution, considering the cohesive nature of nanoparticles. Once the nanoparticle mixture was ready, it was gradually incorporated into the rotary mixer containing the concrete mixture. The entire nanoparticle mixture was systematically added and blended thoroughly with the concrete mixture. Following this

meticulous blending process, the samples underwent preparation and curing in controlled laboratory conditions, aligning with the standards outlined in ASTM C192/C192M-19 (2019).

### 2.3.2 Mechanical properties

After subjecting the rubberized concrete samples blended with varying $TiO_2$ concentrations to a 28-day curing process in water, a series of experimental assessments were performed. For the assessment of compressive strength, three cubical samples (100 mm × 100 mm × 100 mm) were employed per mix. Testing was performed through a 3,000 kN capacity UTM by following BS EN 12390-3 (2009) guidelines. The direct tensile test involved dog-bone-shaped samples sized at 420 mm × 120 mm × 30 mm was tested based on Japan Society of Civil Engineers (2008). This evaluation was performed at a controlled loading rate of 0.15 mm/min via a 200 kN capacity UTM equipped with built-in LVDTs. Real-time test data was collected and processed by a computer, displayed during testing. Additionally, flexural testing was carried out on beam samples measuring 500 mm × 100 mm × 100 mm through UTM apparatus at a loading rate of 0.05 kN/s by confirming BS EN 12390-5 (2009). Each mix underwent testing with three samples, and the average values of the flexural properties were presented based on these tests.

### 2.3.3 Deformation characteristics

The analysis of the modulus of elasticity (ME) was achieved through the static procedure specified in ASTM C469 (ASTM C469, 2002). Every mixture was evaluated utilizing four cylinders (300 mm × 150 mm). Two cylindrical samples were designated for the determination of the CS of the mixture (i.e., the stress and ultimate load), whereas the remaining two were used to ascertain the ME. Linear and lateral deformations were measured using a compressor meter in conjunction with dial gauges affixed to the sample. At the time of this measurement, 40% of the maximal load derived from the compressive experiments was applied to the sample. Eq. (1) was utilized in the computation of the ME.

$$E = \frac{(\sigma_2 - \sigma_1)}{(\varepsilon_2 - 0.000050)} \quad (1)$$

where

$E$ is Young's modulus of elasticity, MPa

$\sigma_2$ is the Stress corresponding to 40% of the ultimate load or ultimate Stress, MPa

$\sigma_1$ is the stress associated with a longitudinal strain of 0.000050, MPa

$\varepsilon_{\sigma_2}$ is the specimen's lateral strain at mid-height at a Stress, $\sigma_2$

The evaluation of shrinkage in rubberized concrete incorporating $TiO_2$ mixes followed ASTM C157/C157M (2008) standard. Specimens with dimensions of 280 × 50 × 30 mm were made for this assessment. Two specimens from each mixture were made for measuring shrinkage. Over the span of 28 days, these samples were regularly measured for length changes using a length comparator. The monitoring technique included observing variations in the density of the specimens unless the difference between two successive measurements decreased to less than 0.5%. This systematic observation allowed for an accurate assessment of the shrinkage behaviour in the rubberized concrete blends containing $TiO_2$.

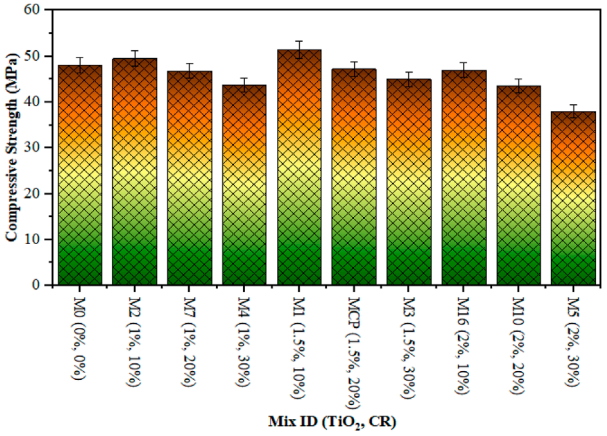


FIGURE 1
CS of rubberised concrete containing $TiO_2$.

### 2.3.4 Durability of rubberised concrete

The evaluation of durability for rubberized concrete incorporating $TiO_2$ involved conducting sorptivity tests and assessing apparent porosity after 28 days. In order to perform the sorptivity test (Jalal et al., 2013), three 30 mm-thick sections were obtained from three CR concrete cubes with dimensions of 100 mm × 100 mm × 70 mm. These cubes had undergone a 28-day curing process. The specimens underwent a drying process in an oven set at 105°C for 24 h and were subsequently cooled in desiccators to ensure uniform conditions. Sidewalls were coated with epoxy resin to prevent water absorption from the sides, enabling absorption solely from the bottom. Placed in pans with tap water at a level 52 mm above the pan's base, the specimens were allowed to absorb water. Regular mass measurements were taken after draining excess water with an absorbent cloth. A plot was generated using the cumulative absorbed volume of water per unit area against the square root of time. The slope of the fitted line to this plot provided the basis for calculating the sorptivity coefficient using Eq. 2 (Nazari and Riahi, 2011c). This coefficient served as a quantifiable measure of water absorption and permeability, contributing to the assessment of durability in the rubberized concrete incorporating $TiO_2$.

$$f_{sc} = \frac{i}{\sqrt{t}} \quad (2)$$

Here,

$fsc$ = coefficient of sorpitivity, mm/√min.,

$i$ = Accumulated water volume per unit area of the surface where water enters, mm and

$t$ = elapsed time, min. For each test, the readings up to 960 s (16 min) were ignored to find the slope of best fitted curve.

To gauge the water absorption capacity of rubberized concrete incorporating $TiO_2$, three cubes from each series underwent a specific procedure. Initially, these cubes were oven-dried for 24 h at 105°C to establish their initial weight, serving as the starting weight for assessment. Subsequently, all of the samples were submerged in water for a period of 24 h to achieve saturation. Subsequently, the final mass of the specimens was measured as the saturated surface's dry weight. The weight loss, measured as a percentage,

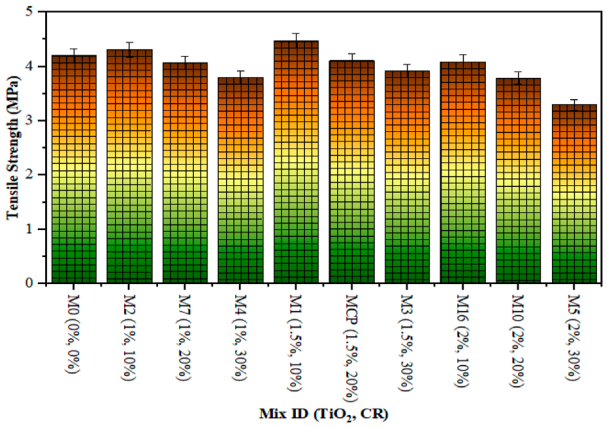


FIGURE 2
TS of Rubberised Concrete containing $TiO_2$.

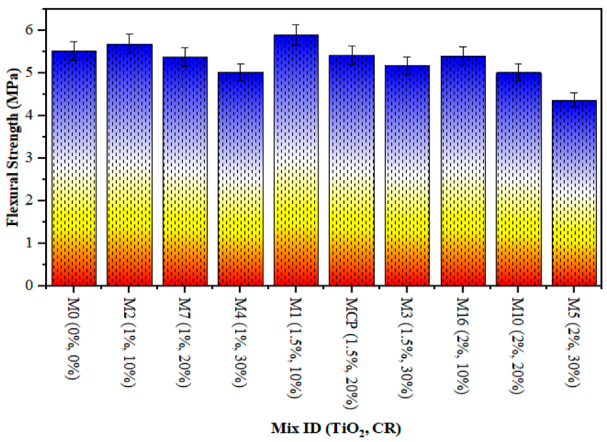


FIGURE 3
Flexural Strength of CR Concrete containing $TiO_2$.

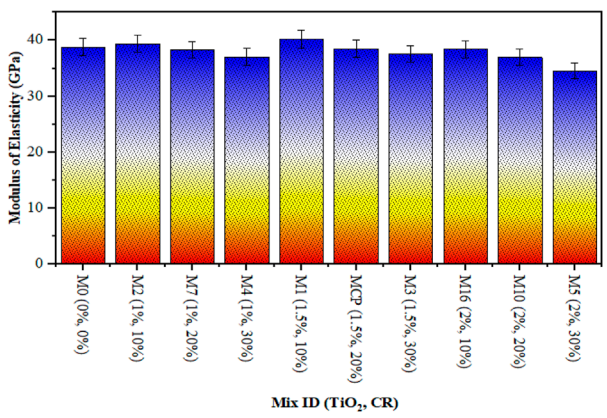


FIGURE 4
ME of Rubberised Concrete containing $TiO_2$.

reflected the degree to which the samples absorbed water (Nazari and Riahi, 2010). It has detected that the specimens were dried at 105°C intentionally to avoid potential microstructural alterations in the $TiO_2$ specimens that higher temperatures might cause, ensuring accurate water absorption measurements (Zhang and Li, 2011). Furthermore, three specimens were utilized to ascertain the apparent porosity (AP). Eq. 3 was applied to calculate AP, providing valuable insights into the material's pore structure and its capacity for water retention.

$$Apparent\,Porosity = \left| \frac{W_i - W_d}{W_i - W_s} \right| \times 100\% \quad (3)$$

Here,
Ww = Mass of the sample after being submerged in water for a duration of 48 h.
Wd = Mass of the specimen after the process of removing moisture by subjecting it to an oven at a temperature of 105°C for a duration of 24 h.
Ws = Mass of the sample while it is suspended in water

# 3 Results and discussions

## 3.1 Compressive strength (CS)

Figure 1 shows how the CS changed at day 28 depending on how much $TiO_2$ nanomaterial was added to different rubberized concrete mixtures. By progressively incorporating CR, the graph organizes mixtures containing an equivalent quantity of $TiO_2$ in each group. The bar graph shows the average of five mixtures that came from the CCD's central points (1.5% $TiO_2$ and 20% CR). This is called MCP. The composition, consisting of a replacement volume of 10% CR for sand and a weight percentage of 1.50% $TiO_2$, achieved an exceptionally high CS of 51.40 MPa. With a sand replacement volume of 30% CR and a weight percentage of 2% $TiO_2$, the minimum CS measured after a period of 28 days was 38 MPa. It is worth mentioning that as CR concentration rises, the graph illustrates a significant drop in the CS of concrete. In line with what Najim and Hall (Nazari et al., 2010). Found, this loss of strength is due to CR not sticking well enough to the cemented cement matrix. Bashar claims that the hydrophobic nature of CR particles, which hinders their ability to combine with water and thereby creates a barrier to bonding, negatively affects the strength of composites. In line with earlier studies (Kundan and Sharma, 2020; Assaggaf et al., 2021; Fauzan et al., 2021). CR makes the composite more fragile because it is weaker and has a lower elastic modulus than microaggregate particles. Prior research (Zhang Z. et al., 2015; Alaloul et al., 2020) stated that the accumulation of CR has a detrimental impact on the CS of composites. These findings corroborate these results. Figure 1 shows that $TiO_2$ can be used as a nanomaterial to strengthen the rubberized concrete matrix, especially when it is mixed with up to 1.5% by weight of Portland cement (PC). The augmentation in $Ca(OH)_2$ absorption is attributed by researchers to the participation of $TiO_2$ in the pozzolanic reaction. The development of C-S-H is facilitated as a result of this hydration procedure acceleration (Wang et al., 2018). Operating as a highly efficient infill, the nanoparticles hinder the unrestricted flow of water vapor within the concrete. Evidently, the CS increased when

1.50 percent $TiO_2$ was incorporated instead of cement but reduced as the proportion of $TiO_2$ increased (Figure 5). Due to two things, the performance has gone down: the nanoparticles are not evenly distributed in the concrete matrix, and there are fewer $Ca(OH)_2$ crystals available, which are needed to make C-S-H gels (Najim and Hall, 2013). Higher concentrations of $TiO_2$ with larger surface areas were also a contributing factor in these samples' excessive water absorption. In line with the work of Rawat et al. (Rawat et al., 2023). Sorathiya et al. (Sorathiya et al., 2018) and Orakzai (Orakzai, 2021), this study found that using 1% nano-$TiO_2$ instead of cement increased the CS by 22.6% after 28 days.

## 3.2 Tensile strength (TS)

The TS is a critical measure of concrete's tensile capacity, impacted by both $TiO_2$ as nanoparticle and CR content as a sand replacement by volume. Figure 2 illustrates the experimental results for rubberized concrete's TS at 28 days, analysed via ANOVA in the RSM framework. The impact of these factors on the TS is statistically evaluated through RSM analysis. The highest recorded tensile strength, at 4.47 MPa, was achieved with 1.50% TiO2 and 10% CR, while the lowest, at 3.30 MPa, occurred with 2% $TiO_2$ and 30% CR replacing sand after 28 days Figure 2 highlights a reducing trend in TS with growing CR content in concrete. Partially substituting sand with CR has a detrimental effect on TS due to water's repulsion on CR, trapping air on its surface, increasing air content in the concrete, and thickening the ITZ between aggregate and PC paste (Khed et al., 2020). This process weakens the bond between PC paste and aggregate. When a load is put on the material, the strain compatibility difference between the hardened state of PC and CR at ITZ causes stress to build up and cracks to form around the CR parts. These cracks have been recognised as weak spots by many studies (Posi et al., 2019; Shaji et al., 2019; Al-Fakih et al., 2020; Shahrul et al., 2021). However, the accumulation of $TiO_2$ as nanoparticle in rubberized concrete showcases a noticeable enhancement in TS. Figure 2 indicates that optimal strength is achieved when $TiO_2$ is up to 1.5%, after which strength begins to decline. This observed enhancement in TS might be accredited to the great surface area of $TiO_2$ nanoparticles, promoting pozzolanic reactions that foster C-S-H gel formation and overall strength increase (Chen et al., 2012). However, further accumulation of $TiO_2$ leads to decreased strength in rubberized concrete, linked to non-uniform nanoparticle dispersion, hindering $Ca(OH)_2$ crystal formation crucial for C-S-H gel development (Khed et al., 2020). Comparable remarks were completed by researchers (Rawat et al., 2023).

## 3.3 Flexural strength (FS)

It is the measure used to quantify the capability of composite to withstand bending. The adhesion between aggregate and PC paste affects the FS (Khed et al., 2020). At the 28-day, the experimental outcomes for rubberized concrete comprising several contents of $TiO_2$ as nanoparticle are illustrated in Figure 3. The material exhibiting the greatest FS noted by 5.91 MPa when composed of 1.5% $TiO_2$ and 10% CR by 28 days. Conversely, the least FS was attained by 4.37 MPa at 2% $TiO_2$ as nanoparticle and 30% CR in place of sand together after 28 days. The trend identified suggests that as CR substitution increases, the FS of concrete declines. The decrease in toughness of CR particles relative to FA which cause of the reduction in FS. In line with this, Sharul et al. (Shahrul et al., 2021) detected that the FS of CR concrete is diminished in comparison to sand particles due to its lesser SG, strength, and load-bearing capacity. Additionally, when sand is replaced with CR, the FS is dropped as a consequence of water repulsion, air entrapment on CR surfaces, and a rise in air content in CR concrete. By increasing the thickness of ITZ that separates aggregate and cement material, their bond is weakened (Khed et al., 2020). The incorporation of $TiO_2$ significantly contributes to the enhancement of FS. As exposed in Figure 3, the FS of PC rises with the $TiO_2$ content reaching 1.5% by weight. The observed improvement can be ascribed to the filling of micropores in rubberized concrete by nanoscale particles of $TiO_2$, which consequently enhance its strength. Nevertheless, as $TiO_2$ continues to accumulate, its strength diminishes as a result of the uneven distribution of particles; this impedes the formation of $Ca(OH)_2$ crystals, which are vital for the development of C-S-H gels (Khed et al., 2020). Scholars have encountered comparable observations (Rawat et al., 2023).

## 3.4 Modulus of elasticity (ME)

The ME, defining concrete's resistance to deformation, is crucial and influenced by multiple features such as concrete's compatibility, aggregate properties, and the ITZ (Silva et al., 2016). The ME test, following ASTM C 469 (ASTM C469, 2002), is strongly correlated with CS and often expressed by empirical equations derived from experimental studies for various concrete types (Alsalman et al., 2017). For rubberized concrete, equations estimating the modulus of elasticity based on various w/c ratios have been developed Figure 4 illustrates the modulus of elasticity results for sixteen experimental runs conducted with rubberized concrete blended with various $TiO_2$ concentrations at 28 days. The highest ME was observed by 40.15 GPa with addition of 1.50% $TiO_2$ and 10% CR, while the lowest ME was noted by 34.52 GPa at 2% $TiO_2$ and 30% CR replacing sand by volume after 28 days respectively. The reduction in ME with increased CR replacement is accredited to the lower stiffness of rubber elements (Khed et al., 2020). However, a noteworthy trend reversal occurred with $TiO_2$ addition. Across all CR replacement levels, mixes containing 1.5% $TiO_2$ exhibited higher ME. This improvement is associated to the nanoscale fineness of $TiO_2$ particles, filling micro pores within rubberized concrete and enhancing its stiffness. Yet, further $TiO_2$ addition led to decreased ME in rubberized concrete. This decline is associated with reduced or unavailable $Ca(OH)_2$ crystals necessary for C-S-H gel formation and non-uniform nanoparticle distribution in matrix (Nazari et al., 2010). These outcomes are dependable with the studies done by Rawat et al. (Rawat et al., 2023).

## 3.5 Drying shrinkage (DS)

It is a significant concern in concrete in which the volume change associated to water loss within the capillary pores of

10.3389/fmats.2024.1357094

TABLE 2 ANOVA outcomes.

| Response | Source | Sum of squares | Df | Mean square | F-value | *p*-value > F | Significance |
|---|---|---|---|---|---|---|---|
| Compressive Strength | Model | 150.47 | 5 | 30.09 | 85.59 | <0.0001 | Yes |
| | A- $TiO_2$ | 25.75 | 1 | 25.75 | 73.23 | <0.0001 | Yes |
| | B-CR | 91.48 | 1 | 91.48 | 260.20 | <0.0001 | Yes |
| | AB | 3.07 | 1 | 3.07 | 8.72 | 0.0145 | Yes |
| | $A^2$ | 27.33 | 1 | 27.33 | 77.74 | <0.0001 | Yes |
| | $B^2$ | 0.14 | 1 | 0.14 | 0.39 | 0.5450 | Yes |
| | Residual | 3.52 | 10 | 0.35 | | | |
| | Lack of Fit | 3.52 | 3 | 1.17 | | | |
| | Pure Error | 0.000 | 7 | 0.000 | | | |
| | Cor Total | 153.98 | 15 | | | | |
| Tensile Strength | Model | 1.16 | 5 | 0.23 | 83.94 | <0.0001 | Yes |
| | A- $TiO_2$ | 0.20 | 1 | 0.20 | 71.52 | <0.0001 | Yes |
| | B-CR | 0.70 | 1 | 0.70 | 254.01 | <0.0001 | Yes |
| | AB | 0.022 | 1 | 0.022 | 8.05 | 0.0176 | Yes |
| | $A^2$ | 0.22 | 1 | 0.22 | 78.40 | <0.0001 | Yes |
| | $B^2$ | 1.074E-003 | 1 | 1.074E-003 | 0.39 | 0.5464 | Not |
| | Residual | 0.028 | 10 | 2.757E-003 | | | |
| | Lack of Fit | 0.028 | 3 | 9.190E-003 | | | |
| | Pure Error | 0.000 | 7 | 0.000 | | | |
| | Cor Total | 1.18 | 15 | | | | |
| | Model | 1.16 | 5 | 0.23 | 83.94 | <0.0001 | |
| Flexural Strength | Model | 1.97 | 5 | 0.39 | 79.57 | <0.0001 | Yes |
| | A- $TiO_2$ | 0.34 | 1 | 0.34 | 67.64 | <0.0001 | Yes |
| | B-CR | 1.20 | 1 | 1.20 | 241.63 | <0.0001 | Yes |
| | AB | 0.039 | 1 | 0.039 | 7.90 | 0.0184 | Yes |
| | $A^2$ | 0.37 | 1 | 0.37 | 73.77 | <0.0001 | Yes |
| | $B^2$ | 1.476E-003 | 1 | 1.476E-003 | 0.30 | 0.5972 | Not |
| | Residual | 0.050 | 10 | 4.956E-003 | | | |
| | Lack of Fit | 0.050 | 3 | 0.017 | | | |
| | Pure Error | 0.000 | 7 | 0.000 | | | |
| | Cor Total | 2.02 | 15 | | | | |

(Continued on the following page)

TABLE 2 (*Continued*) ANOVA outcomes.

| Response | Source | Sum of squares | Df | Mean square | F-value | *p*-value > F | Significance |
|---|---|---|---|---|---|---|---|
| Modulus of Elasticity | Model | 26.26 | 5 | 5.25 | 74.69 | <0.0001 | Yes |
| | A- $TiO_2$ | 4.63 | 1 | 4.63 | 65.92 | <0.0001 | Yes |
| | B-CR | 15.91 | 1 | 15.91 | 226.27 | <0.0001 | Yes |
| | AB | 0.66 | 1 | 0.66 | 9.35 | 0.0121 | Yes |
| | $A^2$ | 4.72 | 1 | 4.72 | 67.17 | <0.0001 | Yes |
| | $B^2$ | 0.011 | 1 | 0.011 | 0.16 | 0.6962 | Not |
| | Residual | 0.70 | 10 | 0.070 | | | |
| | Lack of Fit | 0.70 | 3 | 0.23 | | | |
| | Pure Error | 0.000 | 7 | 0.000 | | | |
| | Cor Total | 26.96 | 15 | | | | |
| Drying Shrinkage | Model | 7.737E-004 | 5 | 1.547E-004 | 2172.79 | <0.0001 | Yes |
| | A- $TiO_2$ | 9.453E-005 | 1 | 9.453E-005 | 1327.36 | <0.0001 | Yes |
| | B-CR | 6.582E-004 | 1 | 6.582E-004 | 9242.15 | <0.0001 | Yes |
| | AB | 4.730E-006 | 1 | 4.730E-006 | 66.42 | <0.0001 | |
| | $A^2$ | 1.564E-007 | 1 | 1.564E-007 | 2.20 | 0.1691 | Not |
| | $B^2$ | 9.898E-006 | 1 | 9.898E-006 | 138.98 | <0.0001 | Yes |
| | Residual | 7.122E-007 | 10 | 7.122E-008 | | | |
| | Lack of Fit | 7.122E-007 | 3 | 2.374E-007 | | | |
| | Pure Error | 0.000 | 7 | 0.000 | | | |
| | Cor Total | 7.744E-004 | 15 | | | | |
| **Sorptivity** | Model | 7.884E-005 | 5 | 1.577E-005 | 129.52 | <0.0001 | Yes |
| | A- $TiO_2$ | 3.977E-005 | 1 | 3.977E-005 | 326.65 | <0.0001 | Yes |
| | B-CR | 4.836E-005 | 1 | 4.836E-005 | 397.20 | <0.0001 | Yes |
| | AB | 1.279E-006 | 1 | 1.279E-006 | 10.51 | 0.0088 | Yes |
| | $A^2$ | 1.308E-006 | 1 | 1.308E-006 | 10.75 | 0.0083 | Yes |
| | $B^2$ | 3.929E-008 | 1 | 3.929E-008 | 0.32 | 0.5825 | No |
| | Residual | 1.217E-006 | 10 | 1.217E-007 | | | |
| | Lack of Fit | 1.217E-006 | 3 | 4.058E-007 | | | |
| | Pure Error | 0.000 | 7 | 0.000 | | | |
| | Cor Total | 8.006E-005 | 15 | | | | |

(Continued on the following page)

TABLE 2 (*Continued*) ANOVA outcomes.

| Response | Source | Sum of squares | Df | Mean square | F-value | *p*-value > F | Significance |
|---|---|---|---|---|---|---|---|
| Apparent Porosity | Model | 57.98 | 5 | 11.60 | 216.12 | <0.0001 | Yes |
| | A- $TiO_2$ | 18.67 | 1 | 18.67 | 347.95 | <0.0001 | Yes |
| | B-CR | 43.55 | 1 | 43.55 | 811.66 | <0.0001 | Yes |
| | AB | 0.96 | 1 | 0.96 | 17.85 | 0.0018 | Yes |
| | $A^2$ | 0.068 | 1 | 0.068 | 1.26 | 0.2878 | Not |
| | $B^2$ | 0.31 | 1 | 0.31 | 5.81 | 0.0367 | Yes |
| | Residual | 0.54 | 10 | 0.054 | | | |
| | Lack of Fit | 0.54 | 3 | 0.18 | | | |
| | Pure Error | 0.000 | 7 | 0.000 | | | |
| | Cor Total | 58.52 | 15 | | | | |

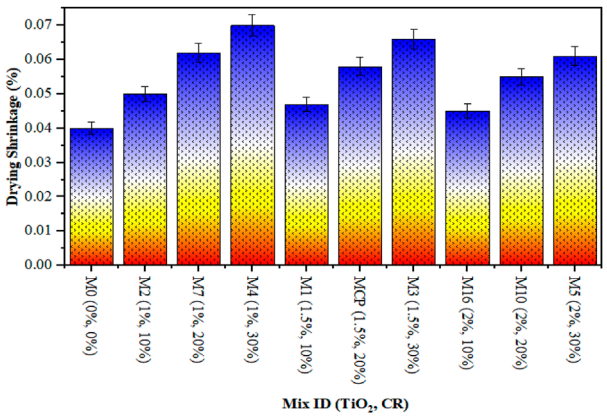


FIGURE 5
DS of Rubberised Concrete comprising $TiO_2$.

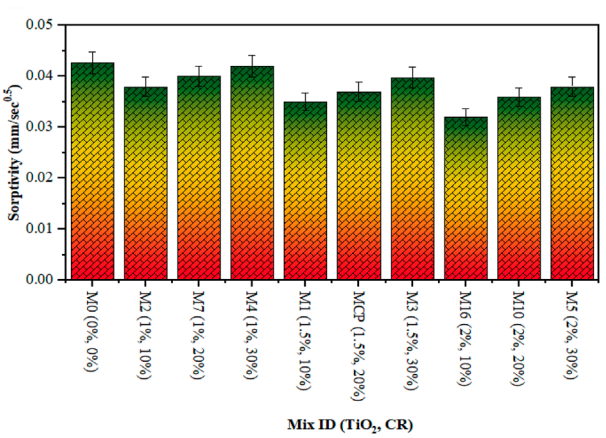


FIGURE 6
Sorptivity of Rubberised Concrete comprising $TiO_2$.

matrix. Figure 5 illustrates a noteworthy decrease in rubberized concrete shrinkage with increasing $TiO_2$ as a nanomaterial addition. The shrinkage values for rubberized concrete blended with $TiO_2$ ranged between 0.05% and 0.066%, higher than the control sample's shrinkage value of 0.04% and the typical composite shrinkage values reported (ranging from $1{,}200 \times 10^{-6}$ to $1800 \times 10^{-6}$) (Zhang et al., 2009). Observations show an increase in concrete shrinkage as the CR content in the mixture rises. This rise is accredited to the lower stiffness of CR constituent part compared to sand, causing increased deformation under drying shrinkage stress (Wang et al., 2019). Also, because CR is flexible, there is less internal restraint within the matrix compared to substituted sand particles. This makes the volume less stable and causes it to shrink more when it dries (Zhang Z. et al., 2015). Moreover, higher CR content leads to improved porosity in the composite owing to the hydrophobic character of CR. This prompts capillary water rise and subsequent volume change upon evaporation, further increasing DS (Huang X. et al., 2013). Adding $TiO_2$ as a nanomaterial to rubberized concrete dramatically decreased its drying shrinkage at all levels of CR replacement, which is a big surprise. This decrease is ascribed to the nanoscale fineness of $TiO_2$ particles, which effectively fill micropores within the mixture. During the concrete drying process, excess water evaporates from the surface, creating an air/water interface within capillary pores. The phenomenon of surface tension creates pressure on the innermost layers of such tiny pores, resulting in an inward push that causes the pore structures to contract and decreases the volume of capillaries. The higher the capillary pores, the greater the potential for concrete to shrink. Nanoparticles are very important for lowering the number of capillary voids, which in turn lowers surface tension and, as a result,

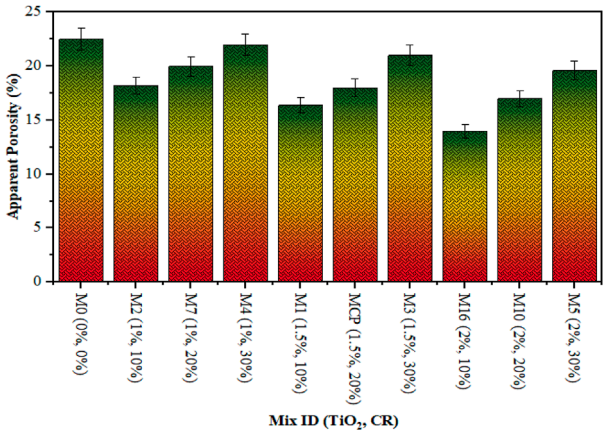


FIGURE 7
Apparent Porosity of Rubberised Concrete comprising $TiO_2$.

lessens the shrinkage that happens when water evaporates from the concrete matrix. Joshaghani (Joshaghani, 2018) noted similar observations.

## 3.6 Sorptivity test

Following a curing period of 28 days, each specimen underwent a sorptivity test in order to evaluate capillary suction. It was possible to determine the slope of the line that links absorption with the square root of time (Nazari, 2011; Saleem et al., 2021). The absorption curve and square root of the absorption coefficient for concrete mixtures are illustrated in Figure 6 (Chen et al., 2012). The provided data illustrates the sorptive outcomes of rubberized concrete mixtures supplemented with varying quantities of $TiO_2$ nanomaterials. After a period of 28 days, the mixture containing 2% $TiO_2$ nanomaterial and 10% CR sand replacement by volume exhibited the lowest sorptivity. The water-only solution exhibited the greatest sorptivity. A higher CR content in concrete is positively correlated with increased sorptivity, according to these findings. This structure forms because rubber is hydrophobic, which raises the capillary water pressure, causes more volume change during evaporation, and then contraction. As a result, a higher CR content leads to more porosity (Huang X. et al., 2013). Notably, adding $TiO_2$ nanoparticles to rubberized concrete greatly decreased its ability to soak up water, no matter how much CR was replaced. The fluctuations in sorptivity levels exhibit a strong correlation with the properties of the pores. $TiO_2$ has a lower sorptivity because its particles are smaller and more C-S-H gel forms, which makes the pores smaller and, in turn, the sorptivity lower (Jayapalan et al., 2009; Zhang R. et al., 2015). When samples with more $TiO_2$ are put into the C-S-H gel, the sorptive levels go down. As a consequence, the interconnection of pores diminishes, resulting in a reduction in absorption. These observations resonate with finding from earlier research (Rawat et al., 2023).

## 3.7 Apparent porosity

Figure 7 illustrates the apparent porosity of rubberized concrete blended with various concentrations of $TiO_2$ as nanomaterial after a 28-day period. Interestingly, the porosity of all concrete including $TiO_2$ was lower than control concrete. However, the porosity of the concrete increased with rising CR content, attributed to the hydrophobic character of CR. This characteristic led to capillary water rise and increased drying shrinkage, thereby augmenting porosity with higher CR content (Huang X. et al., 2013). Conversely, across all CR replacement levels, a significant decrease in porosity was detected upon the introduction of $TiO_2$ as a nanomaterial in rubberized concrete. This decline in porosity can be linked to $TiO_2$ nanoparticles acting as effective fillers. As the nanoparticle conglomerates expanded, the surrounding void spaces were gradually filled. These "nuclei" significantly accelerated hydration rates, leading to reduced porosity as hydration accumulated rapidly within water-filled pores (Mohammadi et al., 2014). Studies by Mohammadi et al. (Mohammadi et al., 2014) showcased reduced total porosity with the substitution of titanium dioxide to calcium phosphate cement. These observations resonate with finding from earlier research by Riahi and Nazari (Nazari and Riahi, 2011b; 2011a), who observed decreased porosity when PC was partially substituted with $TiO_2$ at different concentrations. Their results demonstrated that the decrease in porosity was achieved with a $TiO_2$ content of 3%, showing reductions of 1.64%, 4.3%, 5.67%, and 5.07% in porosity with additions of 1%, 2%, 3%, and 4% $TiO_2$, respectively. Comparable observations were made by other researchers (Zhang and Li, 2011; Jalal et al., 2013; Sorathiya et al., 2018; Rawat et al., 2022).

# 4 RSM analysis

RSM stands out as a powerful statistical and mathematical approach for modelling relationships between independent variables and their corresponding responses. It is widely favoured for its ability to analyse and develop models that effectively capture these connections. Moreover, RSM extends its utility to multi-objective optimization by defining specific goals tied to either the variables or the responses (Adamu et al., 2018). In RSM analysis, several design model types are available, such as CCD models and so on. The selection amongst these options is contingent upon the quantity of factors and the extent of their individual fluctuations (Adamu et al., 2018). Given the unknown mathematical relations between replies and independent factors, the model is often formulated as a linear model represented by a first order function, as shown in Eq. 4.

$$y = \beta_0 + \beta_1 x_2 + \beta_2 x_2 + \beta_n x_n + \epsilon \quad (4)$$

In Equation 5, y characterizes the modelled response. Here, $\beta$ o denotes the $y$-intercept when both X1 and X2 are zero. The coefficients $\beta$ 1 and $\beta$ 2 correspond to the first and second independent factors, correspondingly. X1 and X2 are the coefficients of the first and second factors, correspondingly. The variable 'e' accounts for the error in the model. However, in cases where the data exhibits curvature, a linear model might not be appropriate to capture the response accurately. In such instances, it

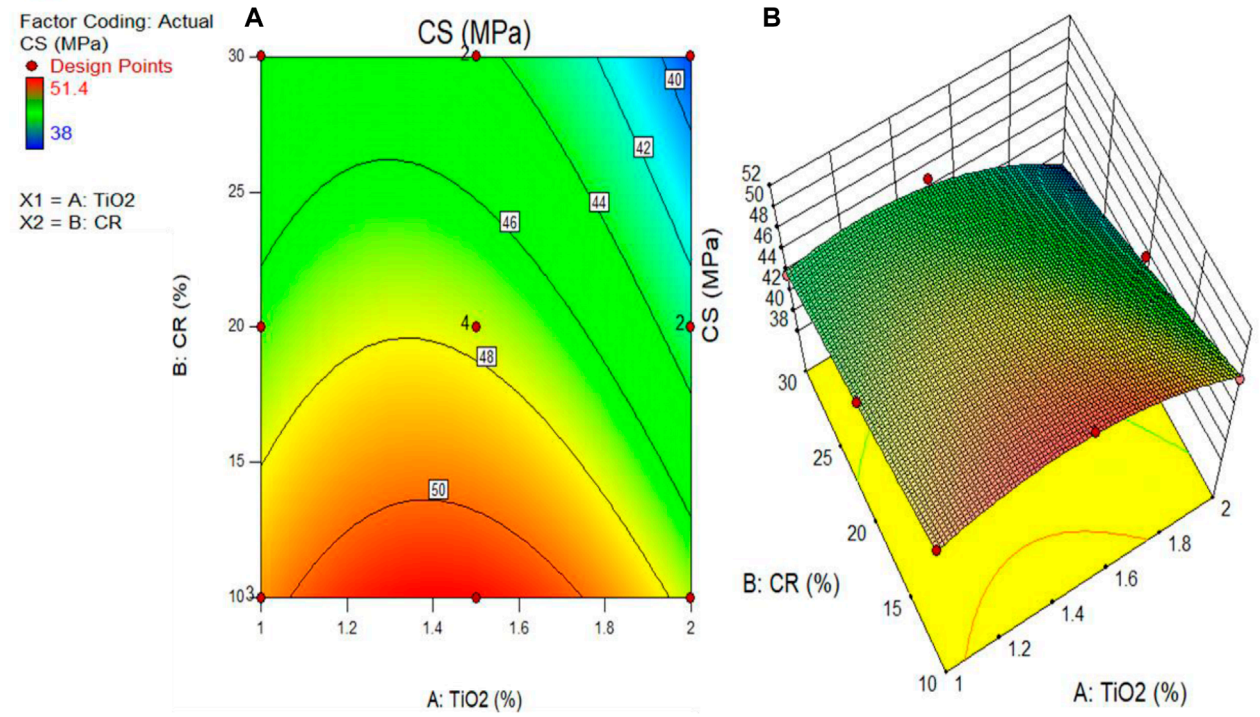


FIGURE 8
**(A)** 2 D contour Diagram and **(B)** 3 D Surface Plots for CS.

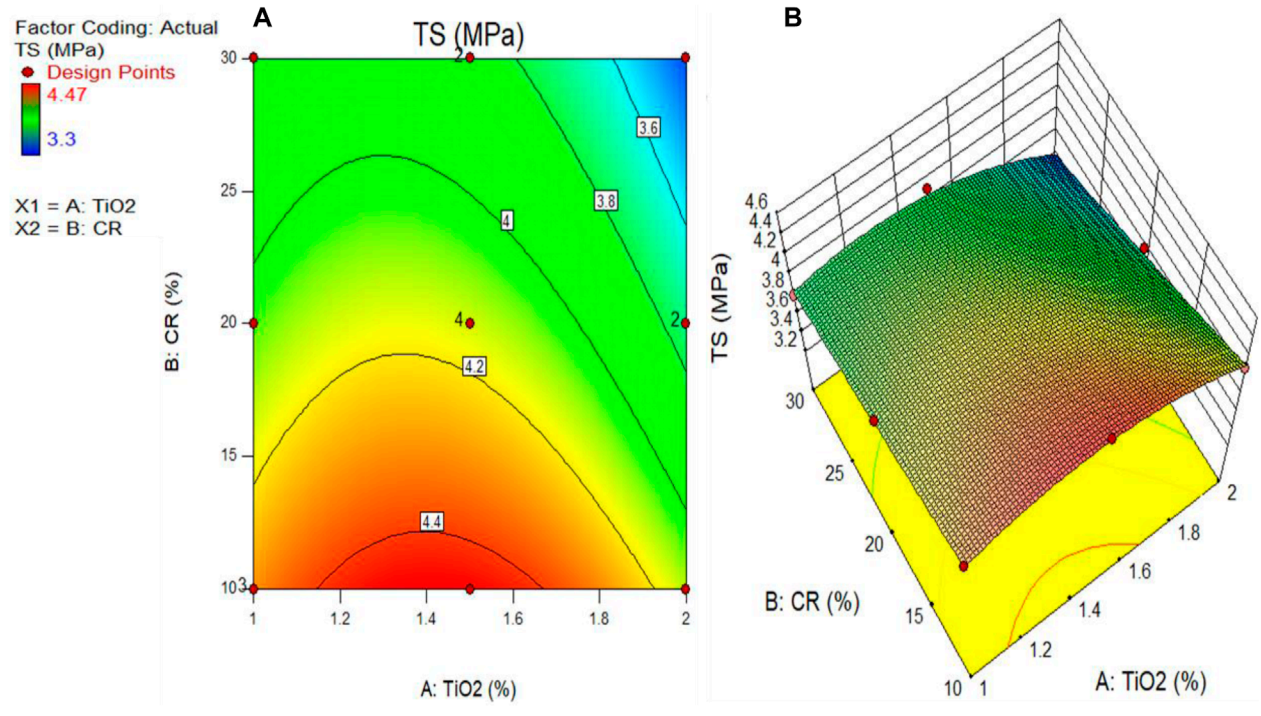


FIGURE 9
**(A)** 2 D contour Diagram and **(B)** 3 D Surface Plots for TS.

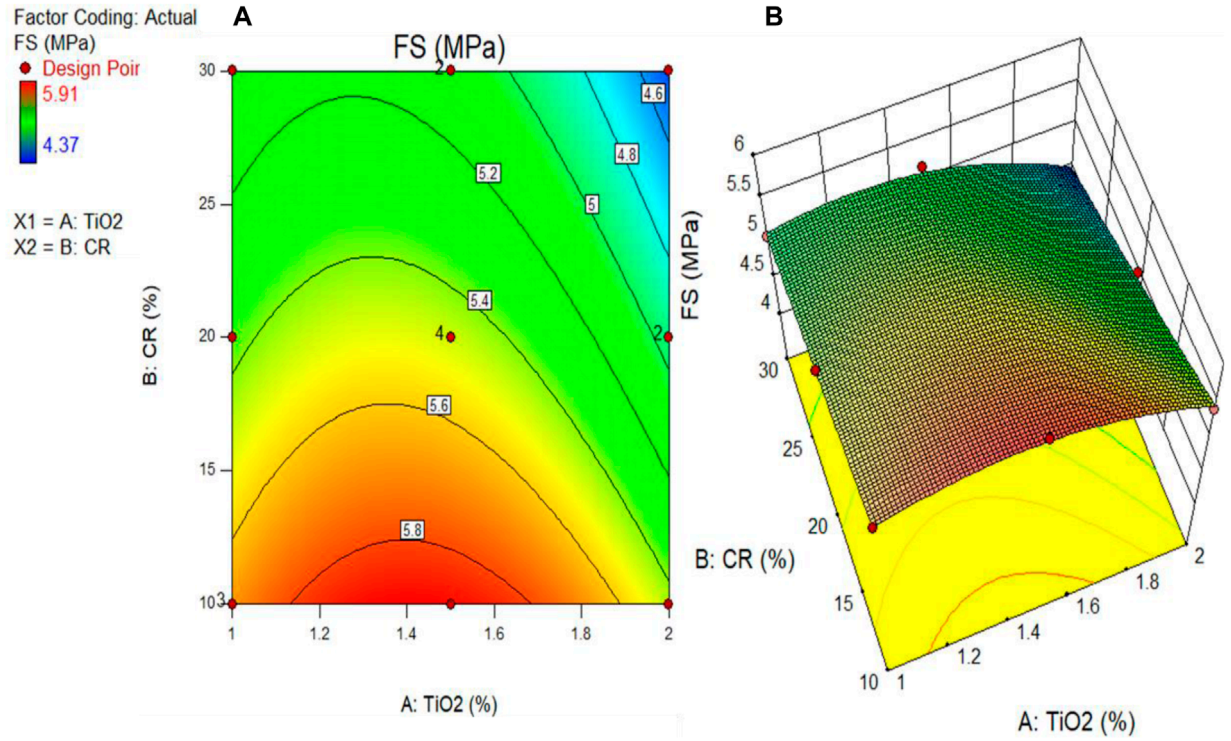


FIGURE 10
**(A)** 2 D contour Diagram and **(B)** 3 D Surface Plots for FS.

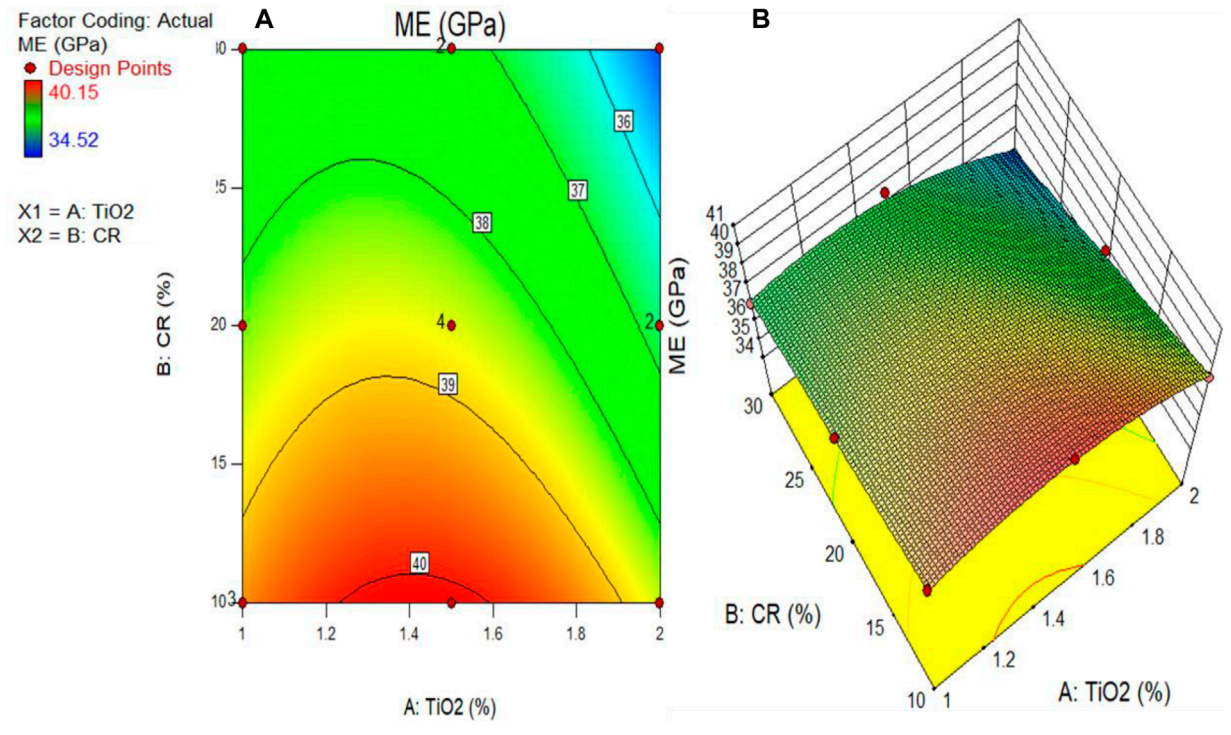


FIGURE 11
**(A)** 2 D contour Diagram and **(B)** 3 D Surface Plots for ME.

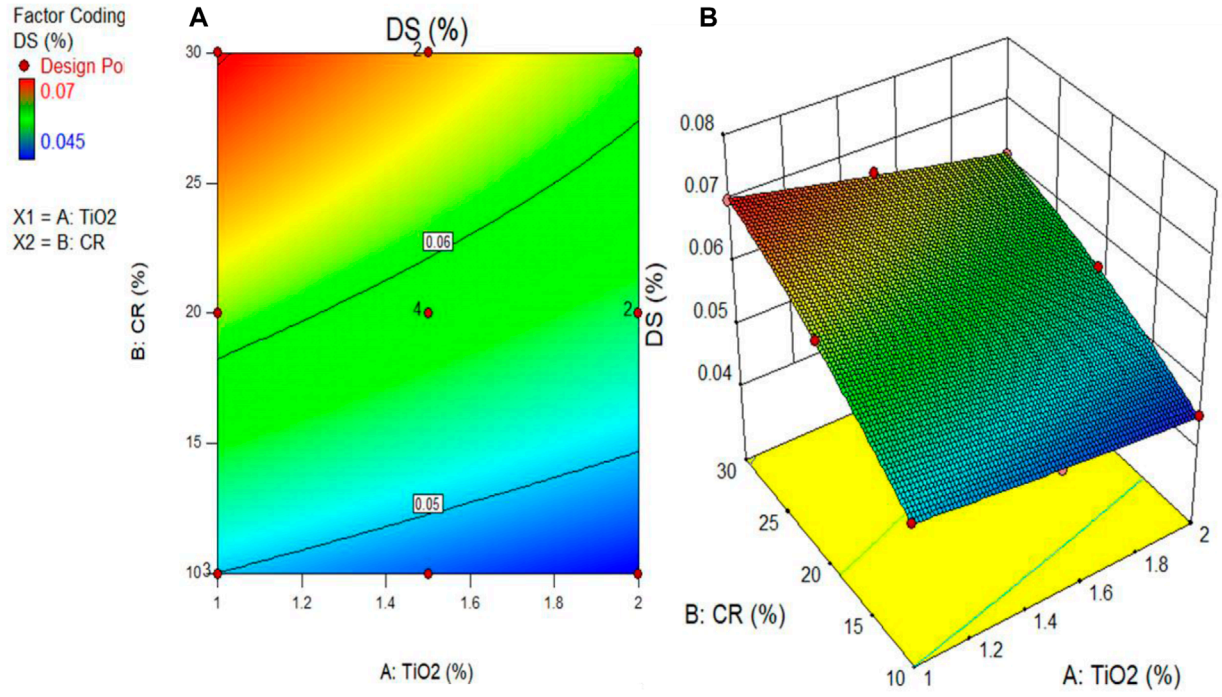


FIGURE 12
**(A)** 2 D contour Diagram and **(B)** 3 D Surface Plots for DS.

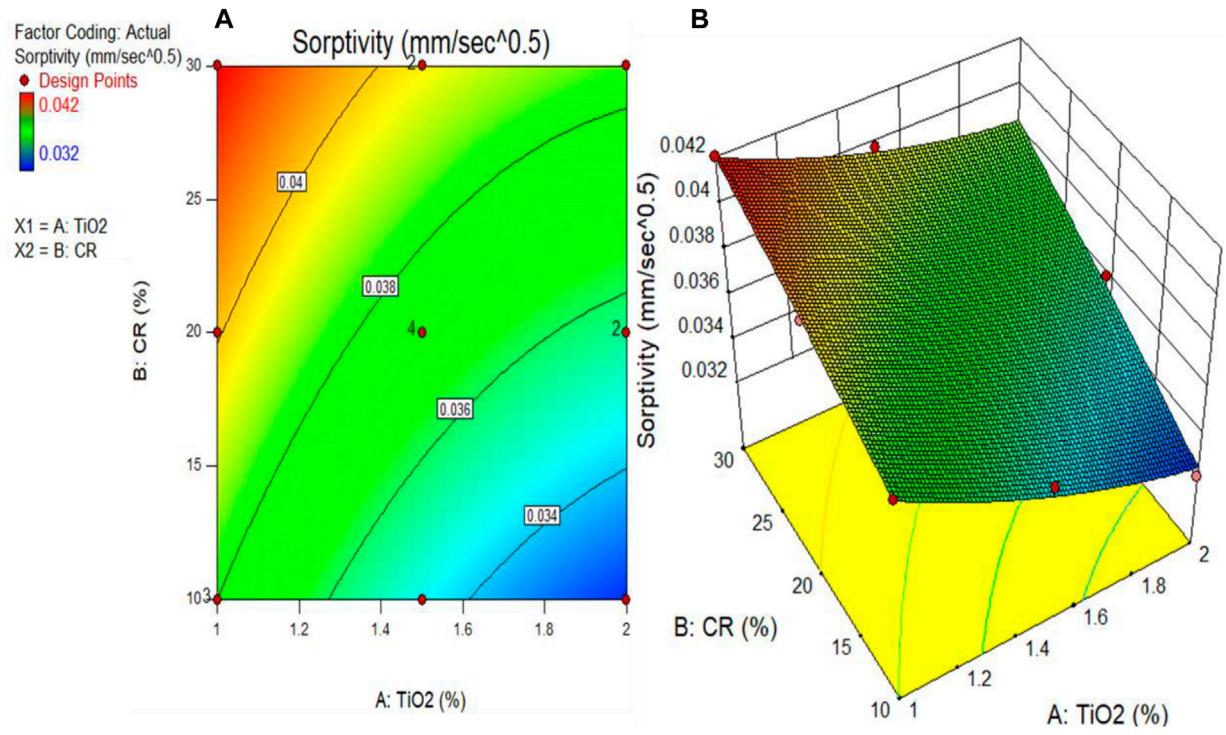


FIGURE 13
**(A)** 2 D contour Diagram and **(B)** 3 D Surface Plots for Sorptivity.

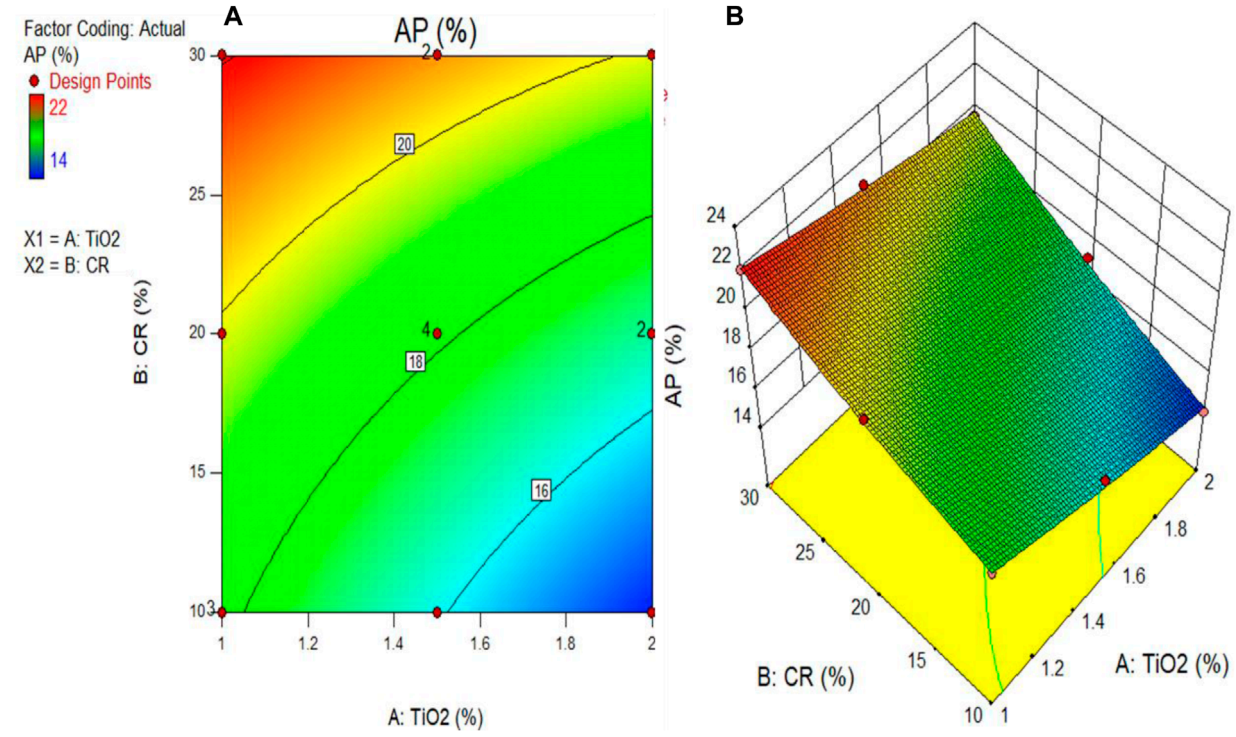


FIGURE 14
**(A)** 2 D contour Diagram and **(B)** 3 D Surface Plots for AP.

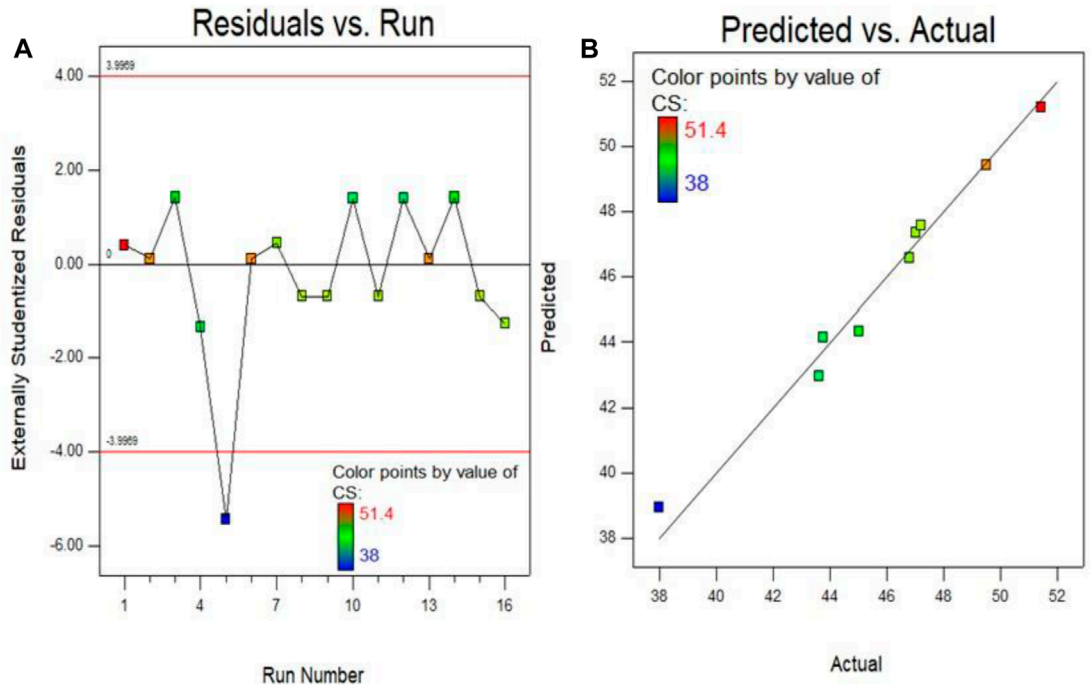


FIGURE 15
**(A)** Residual *versus* Runs plots and **(B)** Predicted against Actual diagrams for CS.

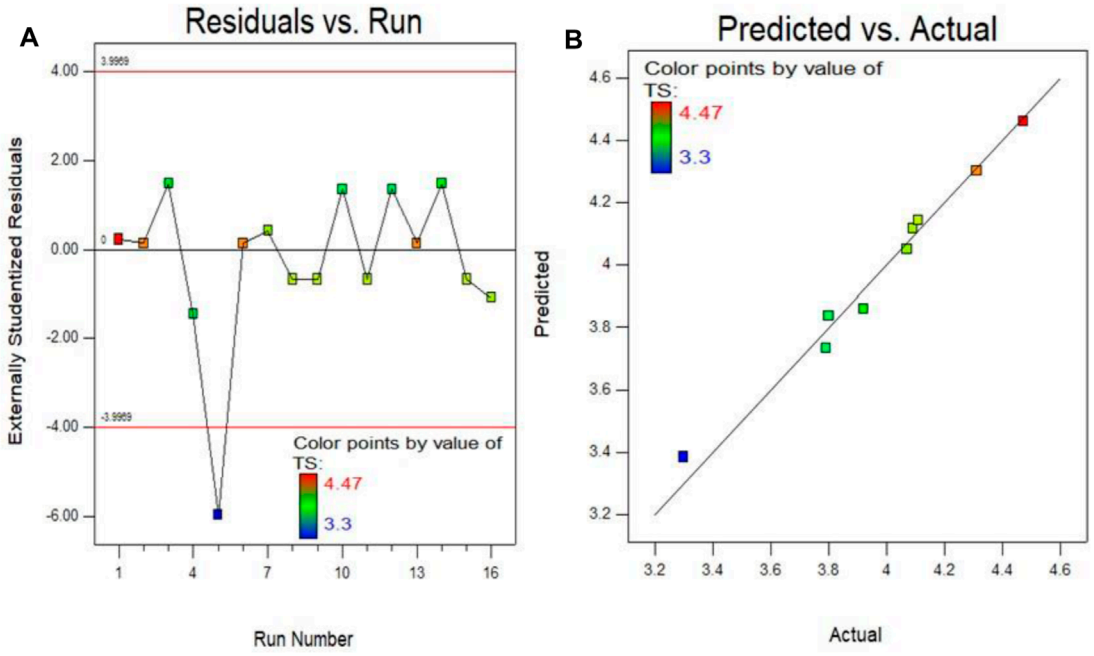


FIGURE 16
**(A)** Residual *versus* Runs plots and **(B)** Predicted against Actual diagrams for TS.

TABLE 3 Model verification parameters.

| Model validation constraints | CS | TS | FS | ME | DS | Sorptivity | AP |
|---|---|---|---|---|---|---|---|
| Standard Deviation | 0.59 | 0.053 | 0.070 | 0.27 | 2.669E-004 | 3.489E-004 | 0.23 |
| Mean | 46.34 | 4.03 | 5.33 | 38.10 | 0.057 | 0.038 | 18.41 |
| C.V. % | 1.28 | 1.30 | 1.32 | 0.70 | 0.47 | 0.93 | 1.26 |
| PRESS | 17.69 | 0.14 | 0.25 | 3.58 | 4.198E-006 | 6.864E-006 | 2.57 |
| −2 Log Likelihood | 21.16 | −56.41 | −47.03 | −4.59 | −225.43 | −216.86 | −8.92 |
| $R^2$ | 0.9772 | 0.9767 | 0.9755 | 0.9739 | 0.9991 | 0.9848 | 0.9908 |
| Adj $R^2$ | 0.9658 | 0.9651 | 0.9632 | 0.9609 | 0.9986 | 0.9772 | 0.9862 |
| Pred $R^2$ | 0.8851 | 0.8821 | 0.8764 | 0.8673 | 0.9946 | 0.9143 | 0.9561 |
| Adeq Precision | 33.815 | 33.478 | 32.629 | 31.814 | 155.424 | 44.555 | 55.271 |
| BIC | 37.80 | −39.78 | −30.39 | 12.04 | −208.80 | −200.22 | 7.72 |
| AICc | 42.49 | −35.08 | −25.69 | 16.74 | −204.10 | −195.52 | 12.42 |

is recommended to employ a higher degree polynomial approach, as depicted by the second order function in Eq. 5.

$$y = \beta_0 + \sum_{i=1}^{k} \beta_i x_i + \sum_{i=1}^{k} \beta_{ii} x_i^2 + \sum_{j=2}^{k} \sum_{i=1}^{j=1} \beta_{ij} x_i x_j + \epsilon \quad (5)$$

Eq. 5 expresses the modelled response, where 'y' signifies the response being modelled. The variables 'xi' and 'xj' represent the coded values of the independent factors. In this context, 'i' denotes the linear coefficient, 'j' signifies the quadratic coefficient, 'β' is the regression constant, 'βo' represents the *y*-intercept when both Xi and Xj are zero, 'k' is the number of variables involved in the analysis, and 'e' accounts for the error (Adamu et al., 2018). The selection of the most suitable model involves considering additional terms and ensuring that the model is not aliased. The highest polynomial from the SMSS is chosen if the supplementary terms are significant. Furthermore, the model summary statistics are examined, and the

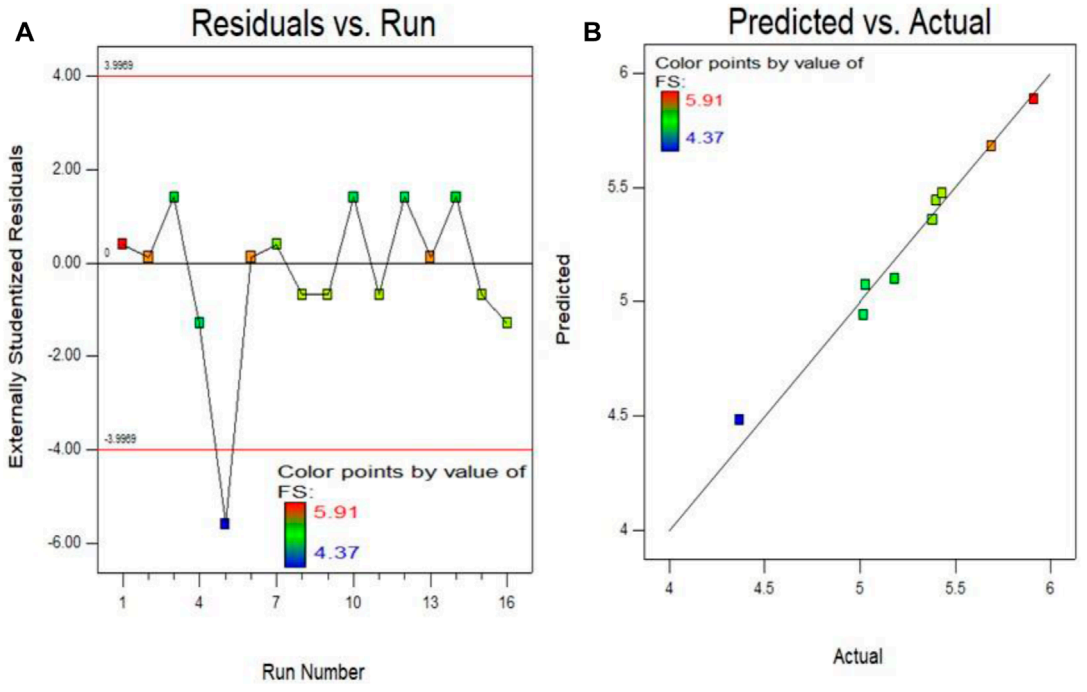


FIGURE 17
**(A)** Residual *versus* Runs plots and **(B)** Predicted against Actual diagrams for FS.

model that increases the predicted and adjusted $R^2$ is selected. The predictive quadratic models for CS, TS, FS, ME, DS, sorptivity and AP were developed, as expressed in Eqs 6–12, utilizing the coded factors $TiO_2$ (A) and CR (B).

$$CS = +47.58 - 1.82 \times A - 3.43 \times B - 0.79 \times AB - 2.80 \times A^2 + 0.20 \times B^2 \quad (6)$$

$$TS = +4.14 - 0.16 \times A - 0.30 \times B - 0.067 \times AB - 0.25 \times A^2 + 0.018 \times B^2 \quad (7)$$

$$FS = +5.47 - 0.21 \times A - 0.39 \times B - 0.089 \times AB - 0.32 \times A^2 + 0.021 \times B^2 \quad (8)$$

$$ME = +38.63 - 0.77 \times A - 1.43 \times B - 0.36 \times AB - 1.17 \times A^2 + 0.057 \times B^2 \quad (9)$$

$$DS = +0.058 - 0.0035 \times A - 0.0092 \times B - 0.00098 \times AB - 0.00021 \times A^2 + 0.0017 \times B^2 \quad (10)$$

$$Sorptivity = +0.037 - 0.0023 \times A + 0.0025 \times B + 0.00051 \times AB + 0.00061 \times A^2 - 0.00011 \times B^2 \quad (11)$$

$$AP = +18.16 - 1.55 \times A + 2.37 \times B + 0.44 \times AB + 0.14 \times A^2 + 0.30 \times B^2 \quad (12)$$

## 4.1 Analysis of variance (ANOVA)

At a 5% significance level (Bheel et al., 2023c; 2023e; 2023f; 2023d), ANOVA was used to look at how the factors interacted with each other and how each parameter affected the responses. Subsequently, any model or term with a *p*-value below 0.05 is deemed significant. The ANOVA findings are shown in Table 2, indicates that all generated models are significant at a significance level of <0.01%. Looking at the specific models, certain terms stand out as significant contributors. For instance, in the CS model, terms A, B, $A^2$, and $B^2$ demonstrate significance. In the meantime, only terms A, B, and $A^2$ are important for the TS, FS, ME, and Sorptivity models. On the other hand, the DS and AP models show significance for terms A, B, and $B^2$. The significance of terms A and B across all models highlights the direct influence of both $TiO_2$ and CR on the responses. Additionally, the significance of $A^2$ and $B^2$ suggests that the quadratic effects of these independent factors also impact the responses. It is important to note that for the interaction between factors to affect the response, the AB term must be significant.

Table 3 showcases the model validation parameters, revealing remarkably high $R^2$ values across all models, fluctuating from 97% to 99.08%. These values signify the strong alignment between the models and the actual data. Additionally, the models exhibit a narrow difference (<0.2) between the adjusted $R^2$ and predicted $R^2$, meeting the criteria for a good fit. Additionally, the signal-to-noise ratio, which measures adequacy precision, exceeds the threshold of 0.4, confirming the accuracy of the models' predictions.

## 4.2 Response surface plots and models diagnostics

Figures 8–14 show portray the interactions between input parameters and outputs (responses) through contour plots and 3D

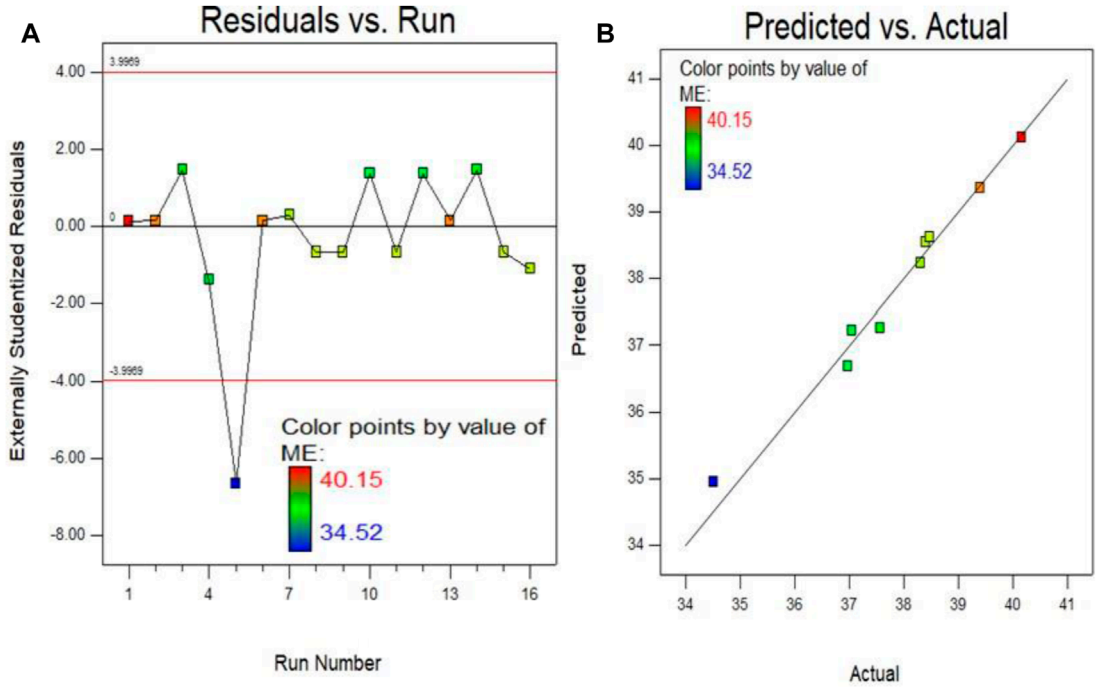


FIGURE 18
**(A)** Residual *versus* Runs plots and **(B)** Predicted against Actual diagrams for ME.

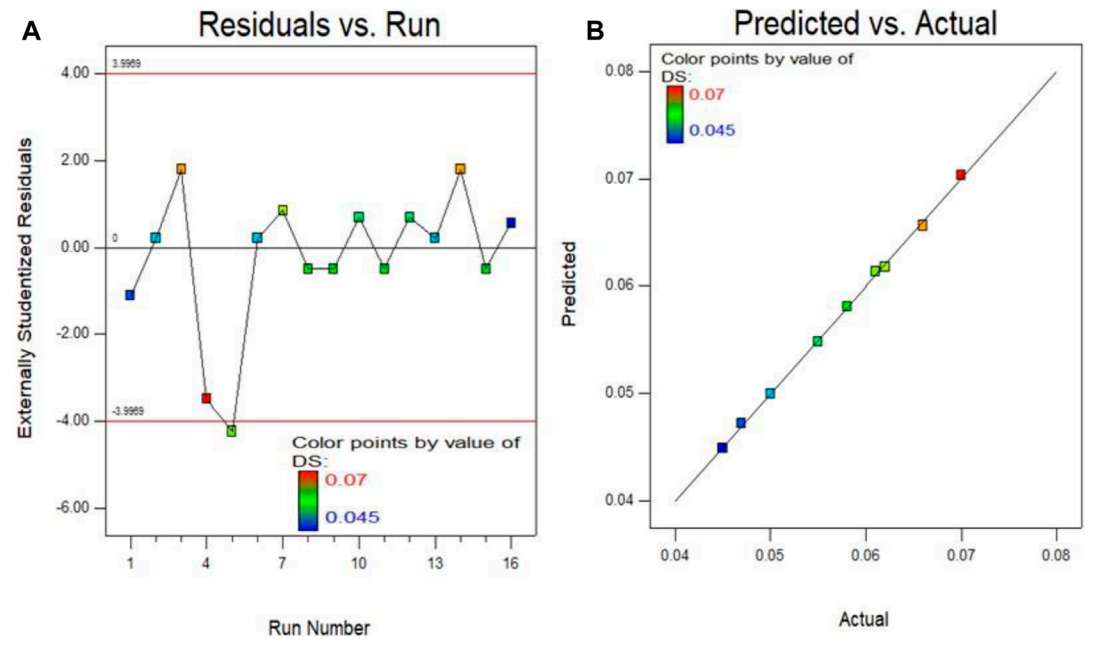


FIGURE 19
**(A)** Residual *versus* Runs plots and **(B)** Predicted against Actual diagrams for DS.

surface plots. They specifically highlight the relationships between different input variables. For instance, Figure 8A,B demonstrate the 2D diagram and 3D plots for CS, showcasing that a significant concentration of CS was observed at a 1.5% $TiO_2$ level in the nanomaterial category among all $TiO_2$ concentrations. Additionally, it is evident that the value of strength notably enhanced when using up to 1.50% $TiO_2$ in the CR concrete. This enhancement can be owing to $TiO_2$'s ability, as a nanomaterial, to fill pores and enhance densification in the CR combination. Similar patterns are observed in the remaining response surface graphs for TS, FS, ME, DS,

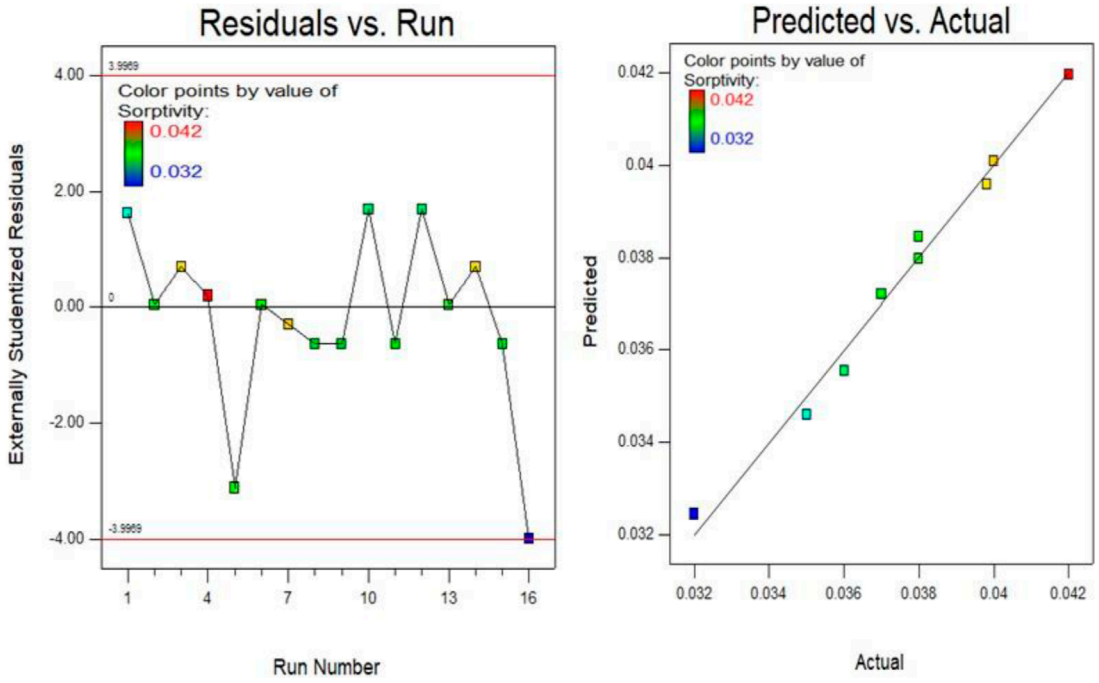


FIGURE 20
**(A)** Residual *versus* Runs plots and **(B)** Predicted against Actual diagrams for Sorptivity.

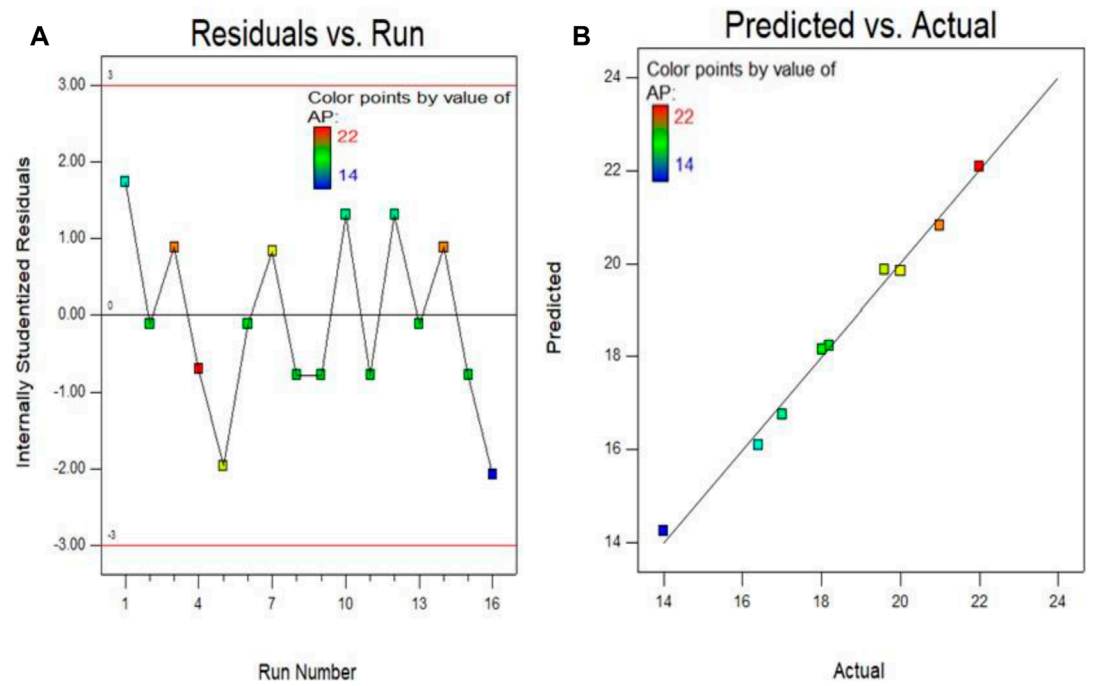


FIGURE 21
**(A)** Residual *versus* Runs plots and **(B)** Predicted against Actual diagrams for AP.

sorptivity, and AP, indicating the impactful relationships between input parameters and outputs.

The RSM evaluation comprises essential diagrams, including crucial model diagnostic graphs like the normal diagram of residuals (Figures 15–21). These graphs, split into (a) run *versus* predicted and (b) real *versus* predicted, serve to validate the significance of the quadratic models used for rubberized concrete with $TiO_2$ as nanomaterials. The plots depict residuals plotted

10.3389/fmats.2024.1357094

TABLE 4 Optimization of outcomes.

| Factors | | Input factors | | Responses (output factors) | | | | | |
|---|---|---|---|---|---|---|---|---|---|
| | | $TiO_2$ (%) | CR (%) | CS (MPa) | TS (MPa) | FS (MPa) | ME (GPa) | DS (%) | Sorptivity (mm/sec$^{0.5}$) | AP (%) |
| Value | Minimum | 1 | 10 | 38 | 3.30 | 4.37 | 34.52 | 0.032 | 0.032 | 14 |
| | Maximum | 2 | 30 | 51.40 | 4.47 | 5.91 | 40.15 | 0.042 | 0.042 | 22 |
| Goal | | Range | Range | Maximize | Maximize | Maximize | Maximize | Minimize | Minimize | Minimize |
| Optimization Results | | 1.59 | 13.74 | 49.47 | 4.31 | 5.69 | 39.41 | 0.051 | 0.035 | 16.48 |
| Desirability | | | | | | 0.661 (66.10%) | | | | |

against the run number (Figures 15–21A), showcasing a consistent distribution without any observable model drift. The data points, encapsulated within red boundary lines, maintain a sinusoidal pattern, affirming the stability of the model throughout the process (Memon et al., 2020). Additionally, the predicted *versus* actual plot (Figures 15–21B) demonstrates strong agreement between experimental and predicted 28-day data for CS, TS, FS, ME, DS, sorptivity, and AP models. The close alignment of distribution points and the minimal variance between experimental and predicted values confirm this agreement. Notably, the points align closely along a straight line, indicating a normal distribution pattern, further validating the model's accuracy.

## 4.3 Multi-objective optimization

It referred to as multi-response optimization is a technique aimed at identifying the most beneficial variables to maximize various responses simultaneously. Real-world optimization problems often involve multiple conflicting objectives, necessitating the search for several optimal solutions (Bheel et al., 2023b; 2023a). Hence, this approach becomes the preferable strategy (Liu et al., 2017; Habibi et al., 2021). Optimization focuses on the model's independent variables, enhancing their efficacy in the process. The objective function guides this optimization, setting the goals for the variables and potentially encompassing significance levels (Liu et al., 2017; MIR et al., 2017). In this process, both independent and dependent variables have objectives established using diverse criteria (Burke and Kendall, 2005; Waqar et al., 2023a). The ultimate aim is to attain objective functions without compromising any of the responses. The desired values, which are between 0 and 1, are what matter in the optimization process for each response, which ranges from 0 to 1 (Waqar et al., 2023b; 2023a; Khan et al., 2023). Elevating the DJ value enhances the favourability of the outcome, often represented as a percentage. In multi-objective optimization, the geometric mean of how desirable each response is found. This lets you find the desirability value of the composite response, which is shown in Eq. 13 (Achara et al., 2019).

$$D = \left(d_1^{r1} \times d_2^{r2} \times d_3^{r3} \times \cdots\cdots\cdots\cdots \times d_n^{rn}\right)^{\frac{1}{n}} \tag{13}$$

In this context, "n" represents the total number of responses considered during the optimization process, while "ri" denotes the assigned weight of significance to each function, ranging from 1 (least important) to 5 (most crucial). In this specific model, the desirability limit was set between 0% and 1%, where a value closer to 1% indicates a more favourable outcome, strengthening the optimized results impact on determining the dependent variable. These parameters outline the optimization goals of the variables. Notably, the optimization aims to maximize the responses for CS, TS, FS, and ME, whereas it aims to minimize responses for DS, sorptivity, and AP. The optimized results indicate maximum values for CS (49.47 MPa), TS (4.31 MPa), FS (5.69 MPa), ME (39.41 GPa), DS (0.051%), sorptivity (0.035 mm/s^0.5), and AP (16.48%), detailed in Table 4. The variability analysis of the model reflects a desirability of 66.10%, indicating the models ability to produce relevant and promising outcomes. These desirability results stem from the optimization method as shown in Table 4.

### 4.4 Model validation

Experimental validation aimed to understand the disparities between the predicted response values derived from the optimization process and the actual experimental values. The optimal parameters, concrete samples were created, incorporating various proportions of CR as a sand substitute alongside $TiO_2$ nanomaterials as cementitious components. The comparison between predicted and experimental values of CS, TS, FS, ME, DS, Sorptivity and AP is expressed as a percentage error, i.e 2.45%, 2.80%, 1.93%, 1.50%, 5.88%, 5.71%, and 4.92% respectively and all responses exhibit an error percentage of less than 6%. This low error percentage across all responses signifies a high level of precision in approach. The discrepancy ($\delta$) between empirical and anticipated readings for individual responses was calculated using Eq. 14, demonstrating the model's precision in predicting outcomes accurately. In essence, this signifies a high degree of consistency between the anticipated and observed values, affirming the model's accuracy.

$$\delta = \left| \frac{\vartheta_E - \vartheta_P}{\vartheta_P} \right| \times 100\% \tag{14}$$

## 5 Conclusion

This research endeavour focuses on exploring the impact of titanium dioxide as nanomaterials on rubberized concrete, specifically delving into its influence on mechanical, deformation, and durability aspects. Drawing insights from the obtained results, the following key conclusions emerge:

- The introduction of titanium dioxide nanoparticles notably enhanced the mechanical attributes of rubberized concrete. The optimum CS, TS, FS, and ME were recorded by 51.40 MPa, 4.47 MPa, 5.91 MPa, and 40.15 GPa when 1.5% $TiO_2$ and 10% CR were added in rubberised concrete after 28 days respectively. After addition of 1.5% of $TiO_2$ along with 10% of CR, these all properties were getting reduced after 28 days respectively.
- The enhancements in the mechanical characteristics of the rubberized concrete stemmed from the uniform distribution of $TiO_2$ nanoparticles. Acting as nucleation sites for cement hydrates, these nanoparticles facilitated improved performance. Their sizable surface area accelerated the hydration rate, effectively contributing to the observed improvements.
- As the content of $TiO_2$ in the mixture increases, both the drying shrinkage and sorptivity of rubberized concrete decrease. These findings validate that water absorption percentage and capillary absorption height diminish with the application of $TiO_2$ nanoparticles. Notably, the ITZ in concrete experiences improvement attributed to the heightened reactivity and the filler effect induced by $TiO_2$ nanomaterial.
  - The integration of $TiO_2$ nanoparticles led to a notable reduction in the apparent porosity of rubberized concrete. Acting as nanofillers, these nanoparticles enhanced the concrete's resistance to water permeability, contributing to this reduction in porosity.
  - Augmenting the fraction of nanoparticles frequently bolsters the durability of the resultant rubberized concrete. This improvement can be linked to the finer particles integrated into the cement mix and the reinforcing filler effect imparted by the nanoparticles.
- Predictive models for responses were formulated and validated through both ANOVA and experimental validation. These models exhibit robustness, boasting high coefficient of determination ($R^2$) values within the range of 97%–99%. Employing multi-objective optimization, we pinpointed the optimal input variable values at 1.50% for $TiO_2$ nanoparticles and 10% for CR. These values were attained with a desirability value of 66.10%, signifying a favourable outcome according to the optimization process.
- Based on the experimental findings, employing 1.5% titanium dioxide as a nanoparticle in rubberized concrete yields optimal results, suggesting its favourable application within the construction industry. This recommendation stems from observed outcomes that highlight its effectiveness in practical construction scenarios.

## 6 Future recommendations

- Extend testing periods beyond 28 days to assess long-term performance and durability of CR concrete blended with $TiO_2$.
  - Optimize the proportion of CR and $TiO_2$ used in high strength concrete in order to achieve the optimal balance between improving characteristics and maintaining structural soundness.
- Expand the scope of assessment to include additional characteristics such as abrasion resistance, chloride ion penetration resistance, and resistance to chemical attack of rubberized concrete inclusion of $TiO_2$ as nanoscale particle.
- Conduct a life cycle assessment to examine the ecological consequences of producing rubberized concrete addition with $TiO_2$ in comparison to conventional concrete.
- Validate laboratory results by conducting field tests on rubberized concrete accumulation with $TiO_2$ as nanoparticle and applying them to real-world building situations to ensure practicality and applicability.

## Data availability statement

The raw data supporting the conclusion of this article will be made available by the authors, without undue reservation.

## Author contributions

GA: Conceptualization, Formal Analysis, Methodology, Resources, Writing–review and editing, Funding Acquisitions. IC: Data curation, Formal Analysis, Software, Writing–review and editing. MA: Methodology, Validation, Visualization, Writing–review and editing. NB: Conceptualization, Data curation, Investigation, Methodology, Writing–original draft, Writing–review and editing. MA: Data curation, Methodology, Software, Writing–review and editing. TN: Formal Analysis, Validation, Visualization, Writing–review and editing. YG: Formal Analysis, Methodology, Validation, Visualization, Writing–review and editing. HA: Conceptualization, Formal Analysis, Methodology, Visualization, Writing–review and editing.

## Funding

The author(s) declare financial support was received for the research, authorship, and/or publication of this article. This work is funded and supported by the Deanship of Scientific Research at Najran University under the Research Priorities and Najran Research funding program grant code (NU/NRP/SERC/12/12).

## Acknowledgments

The authors are thankful to the Deanship of Scientific Research at Najran University for funding this work under the Research Priorities and Najran Research funding program grant code (NU/NRP/SERC/12/12).

## Conflict of interest

The authors declare that the research was conducted in the absence of any commercial or financial relationships that could be construed as a potential conflict of interest.

## Publisher's note

All claims expressed in this article are solely those of the authors and do not necessarily represent those of their affiliated organizations, or those of the publisher, the editors and the reviewers. Any product that may be evaluated in this article, or claim that may be made by its manufacturer, is not guaranteed or endorsed by the publisher.

## References

Abu el-Hassan, K., Hakeem, I. Y., Amin, M., Tayeh, B. A., Zeyad, A. M., Agwa, I. S., et al. (2023). Effects of nano titanium and nano silica on high-strength concrete properties incorporating heavyweight aggregate. *Struct. Concr.* 25, 239–264. doi:10.1002/suco.202300232

Achara, B. E., Mohammed, B. S., and Liew, M. S. (2019). Bond behaviour of nano-silica-modified self-compacting engineered cementitious composite using response surface methodology. *Constr. Build. Mater.* 224, 796–814. doi:10.1016/j.conbuildmat.2019.07.115

Adamu, M., Mohammed, B. S., and Shahir Liew, M. (2018). Mechanical properties and performance of high volume fly ash roller compacted concrete containing crumb rubber and nano silica. *Constr. Build. Mater.* 171, 521–538. doi:10.1016/j.conbuildmat.2018.03.138

Aghamohammadi, O., Mostofinejad, D., Mostafaei, H., and Abtahi, S. M. (2024). Mechanical properties and impact resistance of concrete pavement containing crumb rubber. *Int. J. Geomech.* 24. doi:10.1061/ijgnai.gmeng-7620

Alaloul, W. S., Musarat, M. A., A Tayeh, B., Sivalingam, S., Rosli, M. F. B., Haruna, S., et al. (2020). Mechanical and deformation properties of rubberized engineered cementitious composite (ECC). *Case Stud. Constr. Mater.* 13, e00385. doi:10.1016/j.cscm.2020.e00385

Albano, C., Camacho, N., Reyes, J., Feliu, J. L., and Hernández, M. (2005). Influence of scrap rubber addition to Portland I concrete composites: destructive and non-destructive testing. *Compos. Struct.* 71, 439–446. doi:10.1016/j.compstruct.2005.09.037

Al-Fakih, A., Wahab, M. M. A., Mohammed, B. S., Liew, M. S., Wan Abdullah Zawawi, N. A., and As'ad, S. (2020). Experimental study on axial compressive behavior of rubberized interlocking masonry walls. *J. Build. Eng.* 29, 101107. doi:10.1016/j.jobe.2019.101107

Al-Rbaihat, R., and Al-Marafi, M. N. (2023). Combined effect of silicon dioxide and titanium dioxide nanoparticles on concrete properties. *J. Ecol. Eng.* 24, 319–335. doi:10.12911/22998993/173210

Alsalman, A., Dang, C. N., Prinz, G. S., and Hale, W. M. (2017). Evaluation of modulus of elasticity of ultra-high performance concrete. *Constr. Build. Mater.* 153, 918–928. doi:10.1016/j.conbuildmat.2017.07.158

Amiri, B., Bahari, A., Nik, A. S., Nik, A. S., and Movahedi, N. S. (2012). Use of AFM technique to study the nano-silica effects in concrete mixture. *Indian J. Sci. Technol.* 5, 2055–2059. doi:10.17485/ijst/2012/v5i2.5

Assaggaf, R. A., Ali, M. R., Al-Dulaijan, S. U., and Maslehuddin, M. (2021). Properties of concrete with untreated and treated crumb rubber – a review. *J. Mater. Res. Technol.* 11, 1753–1798. doi:10.1016/j.jmrt.2021.02.019

ASTM, A. (2008). *C157/C157M-08: standard test method for length change of hardened hydraulic-cement mortar and concrete*. West Conshohocken, PA: Annu. B. ASTM Stand., ASTM International.

ASTM C150/C150M-16e1 (2016). *Specification for Portland cement*. West Conshohocken, PA: ASTM International.

ASTM C192/ C192M-19 (2019). *Standard practice for making and curing concrete test specimens in the laboratory*. West Conshohocken, PA: ASTM International.

ASTM C469 (2002). Standard test method for static modulus of elasticity and Poisson's ratio of concrete in compression. Available at: http://portales.puj.edu.co/wjfajardo/mecanicadesolidos/laboratorios/astm/C469.pdf. Assessed on 10 August 2002.

Bahari, A., Berenjian, J., and Sadeghi-Nik, A. (2016). Modification of portland cement with nano SiC. *Proc. Natl. Acad. Sci. India Sect. A - Phys. Sci.* 86, 323–331. doi:10.1007/s40010-015-0244-y

Bahari, A., Sadeghi Nik, A., Roodbari, M., Mirshafiei, E., and Amiri, B. (2015). Effect of silicon carbide nano dispersion on the mechanical and nano structural properties of cement. *Natl. Acad. Sci. Lett.* 38, 361–364. doi:10.1007/s40009-014-0316-6

Bahari, A., Sadeghi Nik, A., Roodbari, M., Taghavi, K., and Mirshafiei, S. E. (2012). Synthesis and strength study of cement mortars containing sic nano particles. *Dig. J. Nanomater. Biostructures* 7, 1427–1435.

Bheel, N., Ali, M. O. A., Shafiq, N., Almujibah, H. R., Awoyera, P., Benjeddou, O., et al. (2023a). Utilization of millet husk ash as a supplementary cementitious material in eco-friendly concrete: RSM modelling and optimization. *Structures* 49, 826–841. doi:10.1016/j.istruc.2023.02.015

Bheel, N., Benjeddou, O., Almujibah, H. R., Abbasi, S. A., Sohu, S., Ahmad, M., et al. (2023b). Effect of calcined clay and marble dust powder as cementitious material on the mechanical properties and embodied carbon of high strength concrete by using RSM-based modelling. *Heliyon* 9, e15029. doi:10.1016/j.heliyon.2023.e15029

Bheel, N., Mohammed, B. S., Abdulkadir, I., Liew, M. S., and Zawawi, N. A. W. A. (2023c). Effects of graphene oxide on the properties of engineered cementitious composites: multi-objective optimization technique using RSM. *Buildings* 13, 2018. doi:10.3390/buildings13082018

Bheel, N., Mohammed, B. S., Ali, M. O. A., Shafiq, N., and Radu, D. (2023d). Effect of graphene oxide as a nanomaterial on the bond behaviour of engineered cementitious composites by applying RSM modelling and optimization. *J. Mater. Res. Technol.* 26, 1484–1507. doi:10.1016/j.jmrt.2023.07.278

Bheel, N., Mohammed, B. S., Liew, M. S., and Zawawi, N. A. W. A. (2023e). Durability behaviours of engineered cementitious composites blended with carbon nanotubes against sulphate and acid attacks by applying RSM modelling and optimization. *Buildings* 13, 2032. doi:10.3390/buildings13082032

Bheel, N., Mohammed, B. S., Liew, M. S., and Zawawi, N. A. W. A. (2023f). Effect of graphene oxide as a nanomaterial on the durability behaviors of engineered cementitious composites by applying RSM modelling and optimization. *Buildings* 13, 2026. doi:10.3390/buildings13082026

Bravo, M., and De Brito, J. (2012). Concrete made with used tyre aggregate: durability-related performance. *J. Clean. Prod.* 25, 42–50. doi:10.1016/j.jclepro.2011.11.066

BS EN 12390-3 (2009). *Testing hardened concrete. Compressive strength of test specimens*. London, United Kingdom: British Standards Institution.

BS EN 12390-5 (2009). *Testing hardened concrete: flexural strength of test specimens*. London, United Kingdom: British Standard Institute.

Bunea, G., Alexa-Stratulat, S. M., Mihai, P., and Toma, I. O. (2023). Use of clay and titanium dioxide nanoparticles in mortar and concrete—a state-of-the-art analysis. *Coatings* 13, 506. doi:10.3390/coatings13030506

Burke, E. K., and Kendall, G. (2005). *Search methodologies: introductory tutorials in optimization and decision support techniques*. Springer. doi:10.1007/0-387-28356-0

Chen, J., Kou, S. C., and Poon, C. S. (2012). Hydration and properties of nano-TiO 2 blended cement composites. *Cem. Concr. Compos.* 34, 642–649. doi:10.1016/j.cemconcomp.2012.02.009

Chohan, I. M., Ahmad, A., Sallih, N., Bheel, N., Ali, M., and Deifalla, A. F. (2023). A review on life cycle assessment of different pipeline materials. *Results Eng.* 19, 101325. doi:10.1016/j.rineng.2023.101325

Chou, L. H., Yang, C. K., Lee, M. T., and Shu, C. C. (2010). Effects of partial oxidation of crumb rubber on properties of rubberized mortar. *Compos. Part B Eng.* 41, 613–616. doi:10.1016/j.compositesb.2010.09.009

Corinaldesi, V., Mazzoli, A., and Moriconi, G. (2011). Mechanical behaviour and thermal conductivity of mortars containing waste rubber particles. *Mater. Des.* 32, 1646–1650. doi:10.1016/j.matdes.2010.10.013

Demir, F., Yesilata, B., Turgut, P., Bulut, H., and Isiker, Y. (2015). Investigation of the effects of pH, aging and scrap tire content on the dissolution behaviors of new scrap tire-concrete mixture structures. *J. Clean. Prod.* 93, 38–46. doi:10.1016/j.jclepro.2015.01.043

Dong, Q., Huang, B., and Shu, X. (2013). Rubber modified concrete improved by chemically active coating and silane coupling agent. *Constr. Build. Mater.* 48, 116–123. doi:10.1016/j.conbuildmat.2013.06.072

Faried, A. S., Mostafa, S. A., Tayeh, B. A., and Tawfik, T. A. (2021). Mechanical and durability properties of ultra-high performance concrete incorporated with various nano waste materials under different curing conditions. *J. Build. Eng.* 43, 102569. doi:10.1016/j.jobe.2021.102569

Fauzan, F., Nur, O. F., Albarqi, K., Melinda, A. P., and Jauhari, Z.Al (2021). The effect of waste tyre rubber on mechanical properties of normal concrete and fly ash concrete. *Int. J. GEOMATE* 20, 55–61. doi:10.21660/2020.77.5737

Feng, D., Xie, N., Gong, C., Leng, Z., Xiao, H., Li, H., et al. (2013). Portland cement paste modified by TiO2 nanoparticles: a microstructure perspective. *Ind. Eng. Chem. Res.* 52, 11575–11582. doi:10.1021/ie4011595

Ganjian, E., Khorami, M., and Maghsoudi, A. A. (2009). Scrap-tyre-rubber replacement for aggregate and filler in concrete. *Constr. Build. Mater.* 23, 1828–1836. doi:10.1016/j.conbuildmat.2008.09.020

Ghanim, A. A. J., Amin, M., Zeyad, A. M., Tayeh, B. A., and Agwa, I. S. (2023). Effect of modified nano-titanium and fly ash on ultra-high-performance concrete properties. *Struct. Concr.* 24, 6815–6832. doi:10.1002/suco.202300053

Guo, Y. C., Zhang, J. H., Chen, G., Chen, G. M., and Xie, Z. H. (2014). Fracture behaviors of a new steel fiber reinforced recycled aggregate concrete with crumb rubber. *Constr. Build. Mater.* 53, 32–39. doi:10.1016/j.conbuildmat.2013.11.075

Habibi, A., Ramezanianpour, A. M., and Mahdikhani, M. (2021). RSM-based optimized mix design of recycled aggregate concrete containing supplementary cementitious materials based on waste generation and global warming potential. *Resour. Conserv. Recycl.* 167, 105420. doi:10.1016/j.resconrec.2021.105420

Huang, B., Shu, X., and Cao, J. (2013a). A two-staged surface treatment to improve properties of rubber modified cement composites. *Constr. Build. Mater.* 40, 270–274. doi:10.1016/j.conbuildmat.2012.11.014

Huang, X., Ranade, R., Ni, W., and Li, V. C. (2013b). On the use of recycled tire rubber to develop low E-modulus ECC for durable concrete repairs. *Constr. Build. Mater.* 46, 134–141. doi:10.1016/j.conbuildmat.2013.04.027

Jalal, M., Fathi, M., and Farzad, M. (2013). RETRACTED: effects of fly ash and TiO2 nanoparticles on rheological, mechanical, microstructural and thermal properties of high strength self compacting concrete. *Mech. Mater.* 61, 11–27. doi:10.1016/j.mechmat.2013.01.010

Japan Society of Civil Engineers (2008). Recommendations for design and construction of high performance fiber reinforced cement composites with multiple fine cracks (HPFRCC). *Concr. Eng. Ser.* 82, 6–10.

Jayapalan, A. R., Lee, B. Y., and Kurtis, K. E. (2009). Effect of nano-sized titanium dioxide on early age hydration of portland cement. *Nanotechnol. Constr.* 3, 267–273. doi:10.1007/978-3-642-00980-8_35

Jo, M., Soto, L., Arocho, M., St John, J., and Hwang, S. (2015). Optimum mix design of fly ash geopolymer paste and its use in pervious concrete for removal of fecal coliforms and phosphorus in water. *Constr. Build. Mater.* 93, 1097–1104. doi:10.1016/j.conbuildmat.2015.05.034

Joshaghani, A. (2018). Evaluating the effects of titanium dioxide (TiO2) and carbon-nanofibers (CNF) as cement partial replacement on concrete properties. *MOJ Civ. Eng.* 4, 29–38. doi:10.15406/mojce.2018.04.00094

Khan, M. B., Waqar, A., Bheel, N., Shafiq, N., Hamah Sor, N., Radu, D., et al. (2023). Optimization of fresh and mechanical characteristics of carbon fiber-reinforced concrete composites using response surface technique. *Buildings* 13, 852. doi:10.3390/buildings13040852

Khed, V. C., Mohammed, B. S., Liew, M. S., and Abdullah Zawawi, N. A. W. (2020). Development of response surface models for self-compacting hybrid fibre reinforced rubberized cementitious composite. *Constr. Build. Mater.* 232, 117191. doi:10.1016/j.conbuildmat.2019.117191

Kundan, P., and Sharma, S. (2020). Rubberized cemented concrete composites: a review. *Mater. Today Proc.* 44, 4838–4842. doi:10.1016/j.matpr.2020.11.696

Li, G., Stubblefield, M. A., Garrick, G., Eggers, J., Abadie, C., and Huang, B. (2004). Development of waste tire modified concrete. *Cem. Concr. Res.* 34, 2283–2289. doi:10.1016/j.cemconres.2004.04.013

Li, G., Wang, Z., Leung, C. K. Y., Tang, S., Pan, J., Huang, W., et al. (2016a). Properties of rubberized concrete modified by using silane coupling agent and carboxylated SBR. *J. Clean. Prod.* 112, 797–807. doi:10.1016/j.jclepro.2015.06.099

Li, Q., Liu, Q., Peng, B., Chai, L., and Liu, H. (2016b). Self-cleaning performance of TiO2-coating cement materials prepared based on solidification/stabilization of electrolytic manganese residue. *Constr. Build. Mater.* 106, 236–242. doi:10.1016/j.conbuildmat.2015.12.088

Liu, J. C., Tan, K. H., and Zhang, D. (2017). Multi-response optimization of post-fire performance of strain hardening cementitious composite. *Cem. Concr. Compos.* 80, 80–90. doi:10.1016/j.cemconcomp.2017.03.001

Loh, K., Gaylarde, C. C., and Shirakawa, M. A. (2018). Photocatalytic activity of ZnO and TiO2 'nanoparticles' for use in cement mixes. *Constr. Build. Mater.* 167, 853–859. doi:10.1016/j.conbuildmat.2018.02.103

Meddah, A., Beddar, M., and Bali, A. (2014). Use of shredded rubber tire aggregates for roller compacted concrete pavement. *J. Clean. Prod.* 72, 187–192. doi:10.1016/j.jclepro.2014.02.052

Memon, A. M., Hartadi Sutanto, M., Napiah, M., Khan, M. I., and Rafiq, W. (2020). Modeling and optimization of mixing conditions for petroleum sludge modified bitumen using response surface methodology. *Constr. Build. Mater.* 264, 120701. doi:10.1016/j.conbuildmat.2020.120701

Meng, T., Yu, Y., Qian, X., Zhan, S., and Qian, K. (2012). Effect of nano-TiO 2 on the mechanical properties of cement mortar. *Constr. Build. Mater.* 29, 241–245. doi:10.1016/j.conbuildmat.2011.10.047

Mir, I., Samo, S., Hussain, T., Ali, I., and Durani, H. A. K. (2017). Influence of convergent section length and angle on performance of supersonic nozzle. *Sindh Univ. Res. J. -Science Ser.* 49, 727–732. doi:10.26692/surj/2017.12.48

Mohammadi, M., Hesaraki, S., and Hafezi-Ardakani, M. (2014). Investigation of biocompatible nanosized materials for development of strong calcium phosphate bone cement: comparison of nano-titania, nano-silicon carbide and amorphous nano-silica. *Ceram. Int.* 40, 8377–8387. doi:10.1016/j.ceramint.2014.01.044

Mohammed, B. S. (2010). Structural behavior and m-k value of composite slab utilizing concrete containing crumb rubber. *Constr. Build. Mater.* 24, 1214–1221. doi:10.1016/j.conbuildmat.2009.12.018

Mohammed, B. S., Anwar Hossain, K. M., Eng Swee, J. T., Wong, G., and Abdullahi, M. (2012). Properties of crumb rubber hollow concrete block. *J. Clean. Prod.* 23, 57–67. doi:10.1016/j.jclepro.2011.10.035

Mohammed, B. S., Awang, A. B., Wong, S. S., and Nhavene, C. P. (2016). Properties of nano silica modified rubbercrete. *J. Clean. Prod.* 119, 66–75. doi:10.1016/j.jclepro.2016.02.007

Mohammed, B. S., Azmi, N. J., and Abdullahi, M. (2011). Evaluation of rubbercrete based on ultrasonic pulse velocity and rebound hammer tests. *Constr. Build. Mater.* 25, 1388–1397. doi:10.1016/j.conbuildmat.2010.09.004

Mostafa, F. E. Z. M., Smarzewski, P., El Hafez, G. M. A., Farghali, A. A., Morsi, W. M., Faried, A. S., et al. (2023). Analyzing the effects of nano-titanium dioxide and nano-zinc oxide nanoparticles on the mechanical and durability properties of self-cleaning concrete. *Mater. (Basel)* 16, 6909. doi:10.3390/ma16216909

Mousavi, M. A., Sadeghi-Nik, A., Bahari, A., Jin, C., Ahmed, R., Ozbakkaloglu, T., et al. (2021). Strength optimization of cementitious composites reinforced by carbon nanotubes and Titania nanoparticles. *Constr. Build. Mater.* 303, 124510. doi:10.1016/j.conbuildmat.2021.124510

Najim, K. B., and Hall, M. R. (2013). Crumb rubber aggregate coatings/pre-treatments and their effects on interfacial bonding, air entrapment and fracture toughness in self-compacting rubberised concrete (SCRC). *Mater. Struct. Constr.* 46, 2029–2043. doi:10.1617/s11527-013-0034-4

Nazari, A. (2011). RETRACTED ARTICLE: the effects of curing medium on flexural strength and water permeability of concrete incorporating TiO2 nanoparticles. *Mater. Struct. Constr.* 44, 773–786. doi:10.1617/s11527-010-9664-y

Nazari, A., and Riahi, S. (2010). The effect of TiO2 nanoparticles on water permeability and thermal and mechanical properties of high strength self-compacting concrete. *Mater. Sci. Eng. A* 528, 756–763. doi:10.1016/j.msea.2010.09.074

Nazari, A., and Riahi, S. (2011a). The effects of TiO2 nanoparticles on physical, thermal and mechanical properties of concrete using ground granulated blast furnace slag as binder. *Mater. Sci. Eng. A* 528, 2085–2092. doi:10.1016/j.msea.2010.11.070

Nazari, A., and Riahi, S. (2011b). RETRACTED ARTICLE: TiO2 nanoparticles' effects on properties of concrete using ground granulated blast furnace slag as binder. *Sci. China Technol. Sci.* 54, 3109–3118. doi:10.1007/s11431-011-4421-1

Nazari, A., and Riahi, S. (2011c). RETRACTED: TiO2 nanoparticles effects on physical, thermal and mechanical properties of self compacting concrete with ground granulated blast furnace slag as binder. *Energy Build.* 43, 995–1002. doi:10.1016/j.enbuild.2010.12.025

Nazari, A., Riahi, S., Riahi, S., Shamekhi, S. F., and Khademno, A. (2010). Influence of Al2O3 nanoparticles on the compressive strength and workability of blended concrete. *J. Am. Sci.* 6, 6–9.

Nik, A. S., and Bahari, A. (2012). Nano-particles in concrete and cement mixtures. *Appl. Mech. Mater.* 110–116, 3853–3855. doi:10.4028/www.scientific.net/AMM.110-116.3853

Nik, A. S., Bahari, A., Ebadi, A. G., Nik, A. S., and Ghasemi-Hamzekolaee, A. (2010). The role of nano particles (Si) in gate dielectric. *Indian J. Sci. Technol.* 3, 634–636. doi:10.17485/ijst/2010/v3i6.16

Onuaguluchi, O., and Panesar, D. K. (2014). Hardened properties of concrete mixtures containing pre-coated crumb rubber and silica fume. *J. Clean. Prod.* 82, 125–131. doi:10.1016/j.jclepro.2014.06.068

Orakzai, M. A. (2021). Hybrid effect of nano-alumina and nano-titanium dioxide on Mechanical properties of concrete. *Case Stud. Constr. Mater.* 14, e00483. doi:10.1016/j.cscm.2020.e00483

Pelisser, F., Zavarise, N., Longo, T. A., and Bernardin, A. M. (2011). Concrete made with recycled tire rubber: effect of alkaline activation and silica fume addition. *J. Clean. Prod.* 19, 757–763. doi:10.1016/j.jclepro.2010.11.014

Posi, P., Kasemsiri, P., Lertnimoolchai, S., and Chindaprasirt, P. (2019). Effect of fly ash fineness on compressive, flexural and shear strengths of high strength-high volume fly ash jointing mortar. *Int. J. GEOMATE* 16, 36–41. doi:10.21660/201.54.4662

Rawat, G., Gandhi, S., and Murthy, Y. I. (2022). A critical assessment on the effect of nano-titanium dioxide on the properties of concrete. *Gradjevinar* 74, 553–560. doi:10.14256/JCE.3291.2021

Rawat, G., Gandhi, S., and Murthy, Y. I. (2023). Durability aspects of concrete containing nano-titanium dioxide. *ACI Mater. J.* 120, 25–36. doi:10.14359/51738490

Rostami, H., Lepore, J., Silverstraim, T., and Zundi, I. (2000). "Use of recycled rubber tires in concrete," in Proceedings of the International Conference on Concrete (Springer), 391–399.

Sadek, D. M., and El-Attar, M. M. (2015). Structural behavior of rubberized masonry walls. *J. Clean. Prod.* 89, 174–186. doi:10.1016/j.jclepro.2014.10.098

Saleem, H., Zaidi, S. J., and Alnuaimi, N. A. (2021). Recent advancements in the nanomaterial application in concrete and its ecological impact. *Mater. (Basel)* 14, 6387. doi:10.3390/ma14216387

Segre, N., and Joekes, I. (2000). Use of tire rubber particles as addition to cement paste. *Cem. Concr. Res.* 30, 1421–1425. doi:10.1016/S0008-8846(00)00373-2

Shahjalal, M., Islam, K., Batool, F., Tiznobaik, M., Zahid Hossain, F. M., Sakil Ahmed, K., et al. (2023). Fiber-reinforced recycled aggregate concrete with crumb rubber: a state-of-the-art review. *Constr. Build. Mater.* 404, 133233. doi:10.1016/j.conbuildmat.2023.133233

Shahrul, S., Mohammed, B. S., Wahab, M. M. A., and Liew, M. S. (2021). Mechanical properties of crumb rubber mortar containing nano-silica using response surface methodology. *Mater. (Basel)* 14, 5496. doi:10.3390/ma14195496

Shaji, R., Ramkrishnan, R., and Sathyan, D. (2019). Strength characteristics of crumb rubber incorporated self-compacting concrete. *Mater. Today Proc.* 46, 4741–4745. doi:10.1016/j.matpr.2020.10.306

Shu, X., and Huang, B. (2014). Recycling of waste tire rubber in asphalt and portland cement concrete: an overview. *Constr. Build. Mater.* 67, 217–224. doi:10.1016/j.conbuildmat.2013.11.027

Silva, R. V., De Brito, J., and Dhir, R. K. (2016). Establishing a relationship between modulus of elasticity and compressive strength of recycled aggregate concrete. *J. Clean. Prod.* 112, 2171–2186. doi:10.1016/j.jclepro.2015.10.064

Sorathiya, J., Shah, S., and Kacha, S. (2018). "Effect on addition of nano "titanium dioxide" (TiO2) on compressive strength of cementitious concrete," in International Conference on Research and Innovations in Science, Engineering (Gujarat, India: Kalpa Publications in Civil Engineering), 219–211.

Thomas, B. S., Gupta, R. C., and Panicker, V. J. (2016). Recycling of waste tire rubber as aggregate in concrete: durability-related performance. *J. Clean. Prod.* 112, 504–513. doi:10.1016/j.jclepro.2015.08.046

Turki, M., Zarrad, I., Bretagne, E., and Quéneudec, M. (2012). Influence of filler addition on mechanical behavior of cementitious mortar-rubber aggregates: experimental study and modeling. *J. Mater. Civ. Eng.* 24, 1350–1358. doi:10.1061/(asce)mt.1943-5533.0000512

Wang, J., Dai, Q., Si, R., and Guo, S. (2019). Mechanical, durability, and microstructural properties of macro synthetic polypropylene (PP) fiber-reinforced rubber concrete. *J. Clean. Prod.* 234, 1351–1364. doi:10.1016/j.jclepro.2019.06.272

Wang, L., Zhang, H., and Gao, Y. (2018). Effect of TiO2 nanoparticles on physical and mechanical properties of cement at low temperatures. *Adv. Mater. Sci. Eng.* 2018, 1–12. doi:10.1155/2018/8934689

Waqar, A., Bheel, N., Almujibah, H. R., Benjeddou, O., Alwetaishi, M., Ahmad, M., et al. (2023a). Effect of Coir Fibre Ash (CFA) on the strengths, modulus of elasticity and embodied carbon of concrete using response surface methodology (RSM) and optimization. *Results Eng.* 17, 100883. doi:10.1016/j.rineng.2023.100883

Waqar, A., Bheel, N., Shafiq, N., Othman, I., Khan, M. B., Mansoor, M. S., et al. (2023b). Effect of volcanic pumice powder ash on the properties of cement concrete using response surface methodology. *J. Build. Pathol. Rehabil.* 8, 17. doi:10.1007/s41024-023-00265-7

Younis, K. H., and Mustafa, S. M. (2018). Feasibility of using nanoparticles of SiO2 to improve the performance of recycled aggregate concrete. *Adv. Mater. Sci. Eng.* 2018, 1–11. doi:10.1155/2018/1512830

Yousefi, A., Allahverdi, A., and Hejazi, P. (2013). Effective dispersion of nano-TiO2 powder for enhancement of photocatalytic properties in cement mixes. *Constr. Build. Mater.* 41, 224–230. doi:10.1016/j.conbuildmat.2012.11.057

Youssf, O., Elgawady, M. A., Mills, J. E., and Ma, X. (2014). An experimental investigation of crumb rubber concrete confined by fibre reinforced polymer tubes. *Constr. Build. Mater.* 53, 522–532. doi:10.1016/j.conbuildmat.2013.12.007

Youssf, O., Swilam, A., and Tahwia, A. M. (2023). Performance of crumb rubber concrete made with high contents of heat pre-treated rubber and magnetized water. *J. Mater. Res. Technol.* 23, 2160–2176. doi:10.1016/j.jmrt.2023.01.146

Zhang, J., Gong, C., Guo, Z., and Zhang, M. (2009). Engineered cementitious composite with characteristic of low drying shrinkage. *Cem. Concr. Res.* 39, 303–312. doi:10.1016/j.cemconres.2008.11.012

Zhang, M. H., and Li, H. (2011). Pore structure and chloride permeability of concrete containing nano-particles for pavement. *Constr. Build. Mater.* 25, 608–616. doi:10.1016/j.conbuildmat.2010.07.032

Zhang, R., Cheng, X., Hou, P., and Ye, Z. (2015a). Influences of nano-TiO2 on the properties of cement-based materials: hydration and drying shrinkage. *Constr. Build. Mater.* 81, 35–41. doi:10.1016/j.conbuildmat.2015.02.003

Zhang, Z., Ma, H., and Qian, S. (2015b). Investigation on properties of ECC incorporating crumb rubber of different sizes. *J. Adv. Concr. Technol.* 13, 241–251. doi:10.3151/jact.13.241

Zhao, L., Guo, X., Ge, C., Li, Q., Guo, L., Shu, X., et al. (2017). Mechanical behavior and toughening mechanism of polycarboxylate superplasticizer modified graphene oxide reinforced cement composites. *Compos. Part B Eng.* 113, 308–316. doi:10.1016/j.compositesb.2017.01.056